WP 1 Living Lab Climate Adaptive Flood Defences Geophysical and geotechnical measurements

Cyrille Fauchard, Griet De Backer, Vincent Guilbert, Lucile Saussaye

Interreg
EUROPEAN UNION
2 Seas Mers Zeeën
Polder2C's
European Regional Development Fund

WP 1 Living Lab Climate Adaptive Flood Defences

Geophysical and geotechnical measurements

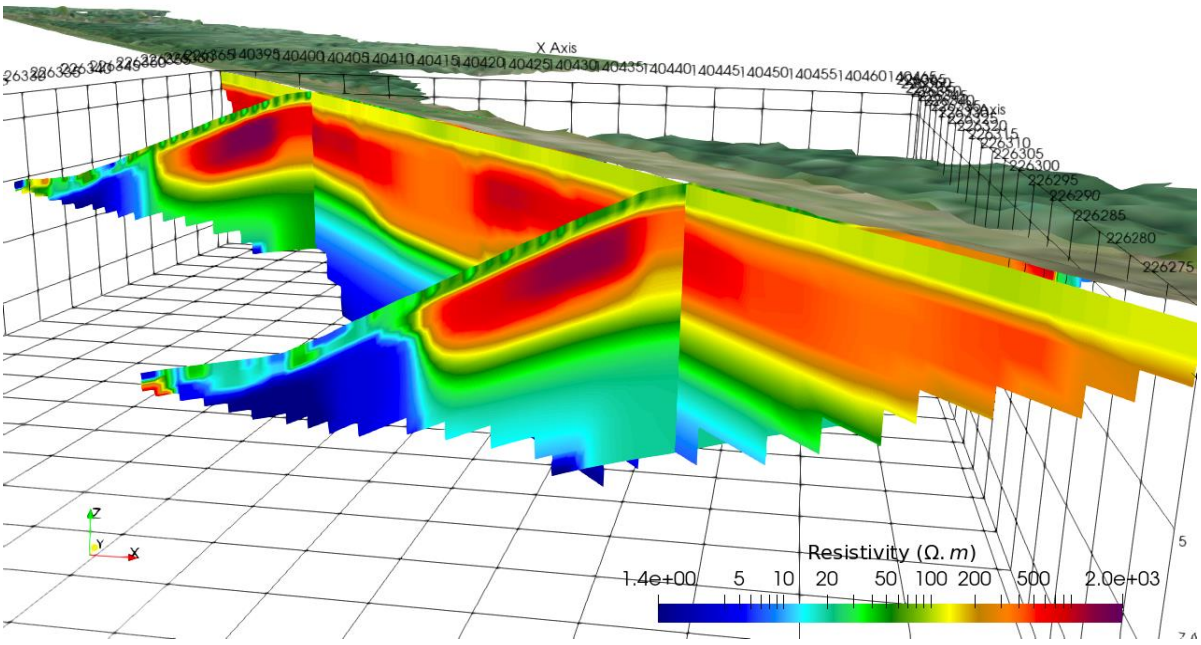

Image: ENDSUM/Cerema

Adaptation to climate change

Interreg 2 Seas Mers Zeeën
Polder2C's
European Regional Development Fund

WP 1 Living Lab Climate Adaptive Flood Defences
Geophysical and geotechnical measurements

Version:
25/01/2023

Authors:
Cyrille Fauchard, Griet De Backer, Vincent Guilbert, Lucile Saussaye

This project has received funding from the Interreg 2 Seas programme 2014-2020 co-funded by the European Regional Development Fund under subsidy contract No [2507-023]

Contents

List of figures

INTERREG Polder2C's project

The INTERREG Polder2C's is an international research project within the framework of the updated Sigmaplan for the river Scheldt. The Hedwige-Prosperpolder will be transformed into tidal nature. Depoldering of Hedwige-Prosperpolder offers a unique testing ground, the Living Lab Hedwige-Prosperpolder, for flood defence and emergency response experts. In this environment current and innovative techniques, processes, methods and products can be tested for practical validation. Thirteen project partners, led by the Dutch Foundation of Applied Water Research (STOWA) and the Flemish Department of Mobility and Public Works (DMOW, Flanders Hydraulics Research), have joined forces. Together, they aim to improve the 2 Seas regions' capacity to adapt to the challenges caused by climate change.

Flood Defence

The rising sea level is a serious threat to the countries in the 2 Seas region. It raises questions as: how strong are our current flood defences?; what is the impact of environmental elements such as the weather, the presence of vegetation or man-made objects on our flood defences? To answer these questions numerous destructive field tests are carried out in the Living Lab to validate flood defence practices. The project entails in-situ testing, guidance on levee maintenance and validation of flood defence infrastructure.

Emergency Response

We aim to improve emergency response by developing the right tools for inspection of water defences, risk evaluation and solutions for flooding. If our water defences do not operate as designed, we must take the right measures to prevent flooding of valuable areas. The Hedwige-Prosperpolder Living Lab offers unique opportunities to exercise emergency management in the event of calamities under controlled but realistic circumstances. Activities that are part of the programme are levee surveillance and monitoring, emergency response exercises, breach initiation and the large European exercise.

Knowledge Infrastructure

We aim to develop a knowledge infrastructure through which existing and new knowledge becomes available and accessible. A necessary success factor for any initiative to improve knowledge is to have its outcomes integrated in practices of a wider community. Knowledge Infrastructure focuses therefore on the consolidation of knowledge acquired in the Living Lab with a variety of activities. Accessibility of data in a user-friendly manner, educational activities in the field and incorporation of knowledge in educational curricula are considered key elements.

Field Station

How can we ensure that both experts in the field and the local public benefit from our project and the learnings about climate change, flood resilience, emergency response and the unique environment of the Hedwige-Prosperpolder? An important and unique way of reaching this goal is realising a Field Station at the project site. It will be used during and after the project for educational purposes, research and as a special meeting place for exclusive occasions.

1 Preamble

1.1 Document purpose

The depoldering of Hedwige-Prosperpolder offers a 6 km^2 Living Lab environment, where current and innovative techniques, processes, methods and products were tested for practical validation. Many experiments, like overtopping tests, wave run up tests, erosion tests, etc. have been carried out on the levee to increase our knowledge on flood resilience. Knowledge about the dike construction and layering of the subsoil is essential for flood risk analyses. The living lab Hedwige Prosperpolder offered the ideal opportunity for testing various techniques to determine the layered structure of levees.
This has led to geophysical and geotechnical surveys to be carried out at the Living Lab Hedwige Prosper Polder (LLHPP), near Antwerp (Belgium). The studied dike crosses the Belgium-Dutch border along the banks of the river Scheldt.

Several CPT's and a number of drillings have been performed on the dike crest by the Geotechnics Division of the Department of Mobility and Public Works (MOW) from the Flemish Government in the period 2019-2021. Monitoring wells were installed through the dike, registering the ground water level continuously. Ground samples were analyzed in the geotechnical laboratory in order to characterize the dike composition. All the results of these tests have been reported in De Backer & D'heer, 2022 and Elgün & De Backer et al., 2019. Classical Electrical Resistivity Tomography (ERT) and Ground Penetrating Radar (GPR) profiles were performed alongside the dike as well as across the dike. At some specific positions, drilling with the Permeafor testing were realized to characterize the soil permeability. These tests have been performed by Cerema between 5th and 9th October 2020.

This report aims to present the interpreted results of the various geophysical and geotechnical techniques and to discuss the effectiveness of the techniques for determining the location of various soil layers in levees. All results are cross-analyzed to assess the dike conditions. In order to better visualize the results, an existing Digital Elevation Model (DEM) is used to insert the geotechnical and geophysical data in. The 3D visualization provides an accurate overview of dike materials, constituting the basement of future experiments of the Polder2C's project. This work has also been compared with the above mentioned geotechnical survey by MOW and a former geophysical survey performed by Fugro (Elgün, 2019 and Elgün & De Backer et al. 2019) one year before.
A part of this work has been presented in June 2021 at the International Archives of the Photogrammetry, Remote Sensing and Spatial Information Sciences (Antoine et al., 2021).

2 Data needs and survey method selection

2.1 Identification of data needs

The diagnosis of flood protection dykes includes different reconnaissance phases (Sharp et al., 2013): First, the collection of archives on the construction and history of the structure is a necessary preliminary step for a good diagnosis, as it allows to quickly identify the type of material used, the type of dike construction, the areas of possible repairs, the presence of anthropogenic anomalies, network, walls, etc.

Second, a geophysical survey is usually carried out with non-destructive methods. These methods are numerous and almost exhaustive lists have already been presented by (Fauchard and Mériaux, 2007), (Sharp et al., 2013). The electrical resistivity imaging method remains the most widely used. It provides an image of the structure, either lengthwise or crosswise, representing the electrical resistivity of the materials, which is related to the distribution and nature of the materials within the structure. A dense literature exists on this topic and the main basis of the method is widely known (Loke, 2004; Telford et al., 1990; Zhdanov and Keller, 1994). The advantage of this method is that it produces internal images of dikes, whether they are made of resistant or conductive materials. The implementation of the method in the field and the time required for measurements can be a constraint, especially if the linear distance to be surveyed is large. Example of measurements on dikes are also numerous (Dezert et al., 2019; Hennig et al., 2005). Some advances in dike survey with ERT method proposed to take into account for 3D effects, since the slope of the dike may have an influence on inversed profiles, such as depicted by (Fargier et al., 2014; Marescot et al., 2006; Rücker et al., 2006).

The production of internal images of the structures is a first step in assessing the distribution of materials, the presence of anomalies and the overall homogeneity of the embankment. Nevertheless, geophysical methods do not provide direct information on the nature of the materials. For this purpose, geotechnical methods are used: (i) the Permeafor is an instrument that allows the permeability of the soil to be assessed during drilling, every 20 cm. It was developed by (Reiffsteck et al., 2010) and successfully used combined with ground penetrating radar measurement (GPR) for dike assessment by (Antoine et al., 2015). (ii) The Cone Penetrating Test (CPT) is the second geotechnical method performed in this study. A description of the CPT method can be found in (Liao et al., 2002) These two methods make it possible to specify the stratigraphy of the soils and certain mechanical properties: the tip resistance (q_c) and its corrected value (q_t), the sleeve friction (interface friction between the penetrometer and soil) and the pore pressure (u) allow to determine the subsurface layering, soil type, and strength properties. The nature of materials is determined by destructive sampling, such as augering or core drilling.

In a first section, we present the ERT, the GPR, the Permeafor as well as the CPT's and drillings, previously reported by (Griet De Backer and Stefanie D'heer, 2022) in the context of Polder2C's project) carried out on a portion of the polder, representing a dike of more than 3.65 km in length. In a second section, the comparison of two ERT measurement campaigns (by Fugro in 2019 and by Cerema in 2020) is proposed. Finally in a third section, we show the results of a 3D inversion taking account for the topography of the section 4, based on the four ERT profiles. The topography was obtained by drone photogrammetric techniques (Pierrot-Deseilligny and Clery, 2012).

2.2 Living Lab Hedwige-Prosper Polder dikes

The LLHPP is a polder located in the Belgian-Dutch border, Northwest of Antwerp, facing the Scheldt river (Dutch: Schelde) at Doel. The dikes were built to protect the polder from high tides and is now a living laboratory where various erosion tests are scheduled in the context of the Polder2C's project. Its location is shown in Figure 1. By convention in this work, all geographic coordinates are given in the Belgian Lambert 72 system (EPSG: 31370).

Figure 1: Location of Living Lab Hedwige-Prosper Polder in the Belgian-Dutch border

The area studied in the context of the project represents a 3.65 km long dike, divided into eleven sections where various experiments (internal and external erosion, overtopping, etc.) have been conducted. Our survey consists of geophysical (ERT and GPR) and geotechnical measurements with Permeafor on four sections, namely the sections 4, 6, 10 and 11. CPT's were formerly made in March and April 2019 on the same sections. A global aerial view of the site with measurement points, profiles and relevant section numbers is given in the Figure 2, completed with the orthoimage obtained by photogrammetry previously performed by drone.

Figure 2: Satellite Google map view of LHPP, the UAV orthophoto obtained thanks to photogrammetry and the sections studied in the context of the Polder2C's project

3 Methodology

3.1 Electrical Resistivity Tomography

Thirteen ERT profiles have been measured with a Terrameter LS2 (©ABEM) and a set of cables and inox electrodes. The method consists of injecting a direct current in the soil with a pair of electrodes and measuring the voltage with another pair of electrodes. The apparent resistivity is then deduced by building a direct model (with finite elements of finite difference) and an inversion consisting of minimizing the calculated potential with the measured one.

A set of electrodes (in this study, 64 or 128 electrodes) are positioned alongside a profile and the space interval is fixed. The length of the profile is related to the depth of investigation (DOI) of the method, while the space interval indicates its resolution. Various configurations of current injection and voltage measurement exist and define a protocol. In this study, the acquisition followed a Schlumberger protocol. Roll-along technique was also used to achieve the longest profiles on sections 4 and 6.

- 2 longitudinal and 3 transverse profiles on section 4;
- 2 longitudinal and 3 transverse profiles on section 6;
- 1 longitudinal and 1 transverse profile on section 10;
- 1 transverse profile on section 11.

The ERT profiles location is shown in the Figure 3, Figure 4 and Figure 5

Technical details are provided in the Table 1.

Table 1 : Characteristics of ERT profiles

Section	Names	Direction **T**ransverse **L**ongitudinal	Nb electrodes	Electrode spacing (m)	Length (m)	Valid Quadripoles	DOI (m)
4	ERT_L1_S4	L	224	3	669	4732	28.7
	ERT_L2_S4	L	96	3	285	1719	28.7
	ERT_T10_S4	T	64	1	63	1062	9.8
	ERT_T11_S4	T	64	1	63	1062	9.6
	ERT_T12_S4	T	64	1	63	1060	9.6
6	ERT_L1S6	L	64	2	125	1060	18.2
	ERT_T21S6	T	57	1	63	768	9.6
	ERT_T22S6	T	56	1	63	732	9.6
	ERT_L2S6N	L	64	2	126	1054	18.2
	ERT_T23S6	T	55	1	63	614	9.6
10	ERT_L1S10	L	64	2	126	1062	18.2
	ERT_T24S10	T	64	1	62	1032	9.6
11	ERT_T25S11	T	64	1	63	1062	6.6

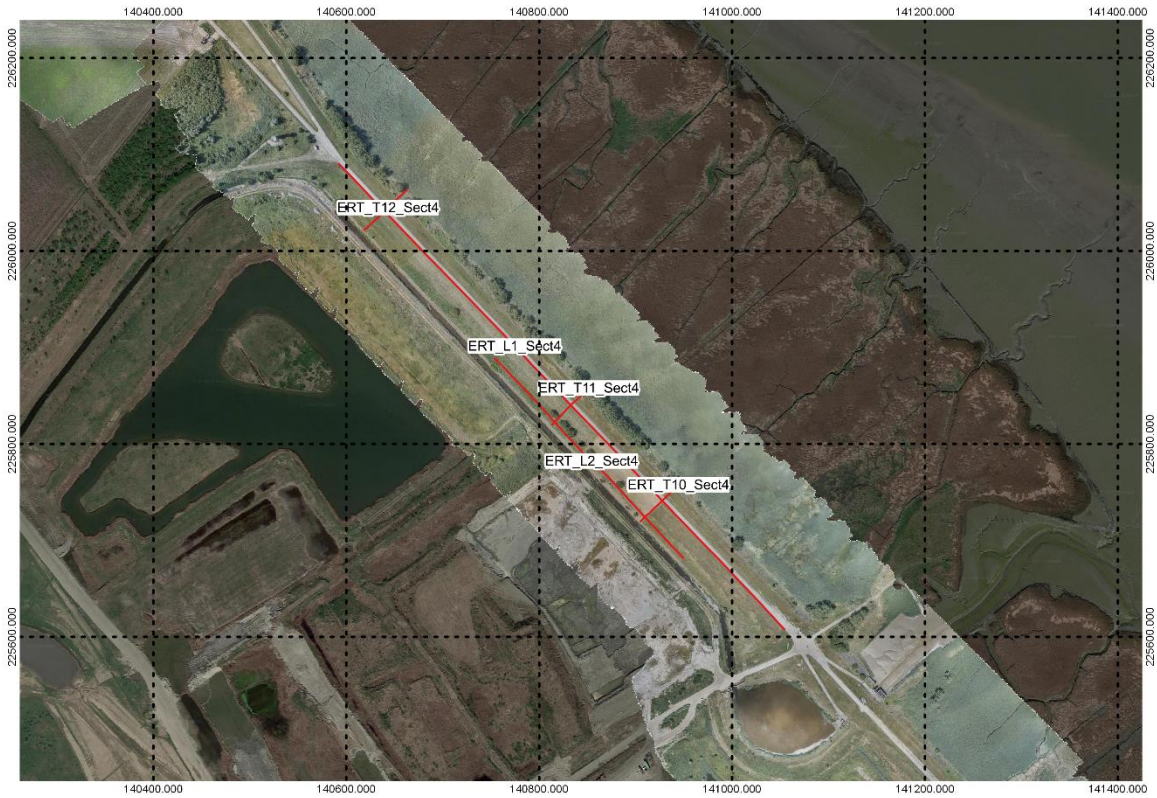

Figure 3: ERT profiles location of section 4

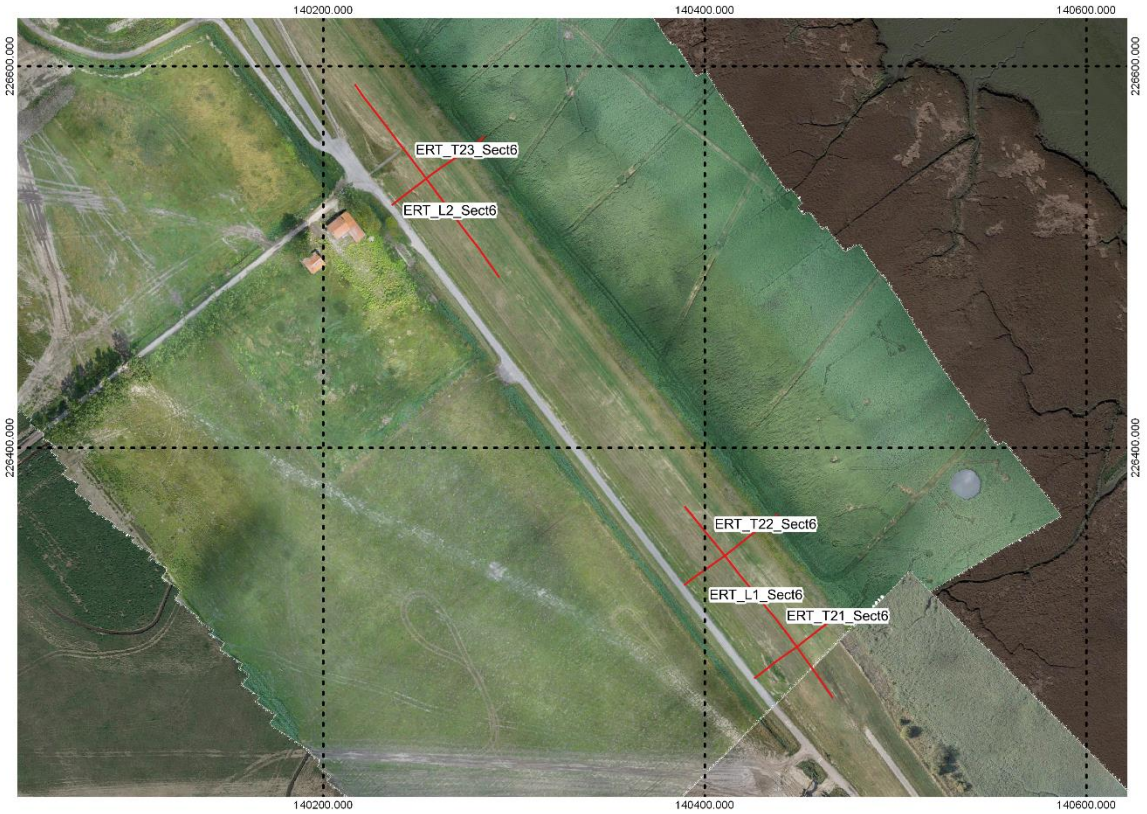

Figure 4: ERT profiles location of section 6

Figure 5: ERT profiles location of sections 10 and 11

3.2 Ground Penetrating Radar

A SIR 3000 GPR system and a 200 MHz bowtie antenna (©GSII) were applied to profiles corresponding to the ERT profiles location of sections S4 and S6. Meteorological conditions unfortunately didn't allow to perform GPR measurements on sections S10 and S11. The location of GPR profiles are shown in the Figure 6 and Figure 7.

The GPR principle is based on the emission and reception of electromagnetic waves propagating in the ground: In our case, a ground-coupled antenna emits an electromagnetic pulse in the time domain down to the ground. Each time this pulse encountered a dielectric contrast at an interface between two materials, a refracted part of the energy continues to propagate deeper while a reflected part propagates to the surface and is measured. The results is called a A-scans, representing the amplitude of the pulse in function of the time of propagation in the soil. The measurement is repeated alongside a profile and we obtain a B-scan (2D image), representing the amplitude of the pulse in color scale in function of the time and propagation and the distance along the profile.

Table 2 shows the characteristics (sections, profiles names, direction transverse or longitudinal to the dike, the depth of investigation (DOI), and the speed of electromagnetic waves applied to perform classical signal processing (surface alignment, Butterworth filtering, background removal, gain adjustment, depth estimation).

Table 2 : Main characteristics of GPR profiles.

Section	Names	Direction **T**ransverse **L**ongitudinal	Length (m)	DOI (m)	Speed (m/ns)
4	GPR_L1S4_C6	L	656	8.45	0.1224
	GPR_L1S4C7	L	656	8.45	0.1224
	GPR_T12S4	T	44	8.45	0.1224
	GPR T11S4	T	43	8.45	0.1224
	GPR_T10S4	T	45	8.45	0.1224
6	GPR_L1S6	L	456	8.45	0.1224
	GPR_T23C9	T	21	8.45	0.1224
	GPR_T23C10	T	42	8.45	0.1224
	GPR_T22S6	T	39	8.45	0.1224
	GPR_T21S6	T	44.5	8.45	0.1224

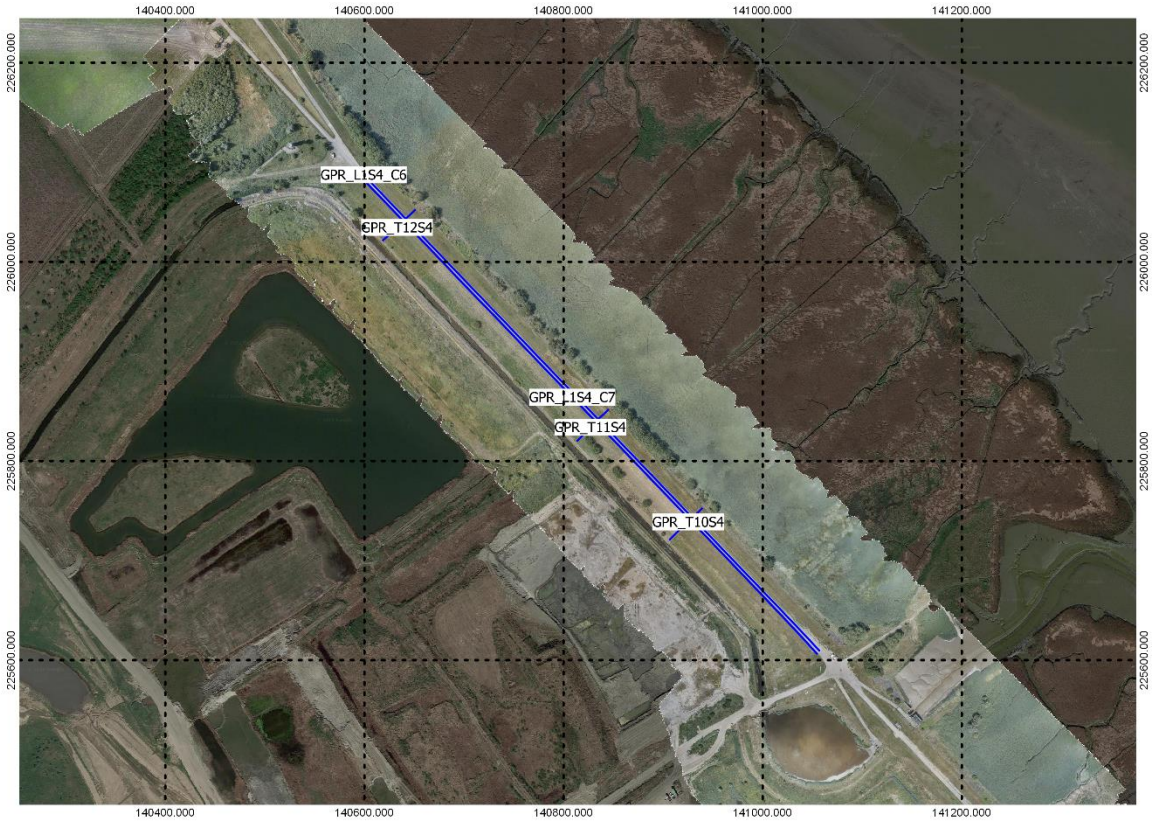

Figure 6: GPR profiles location of section 4

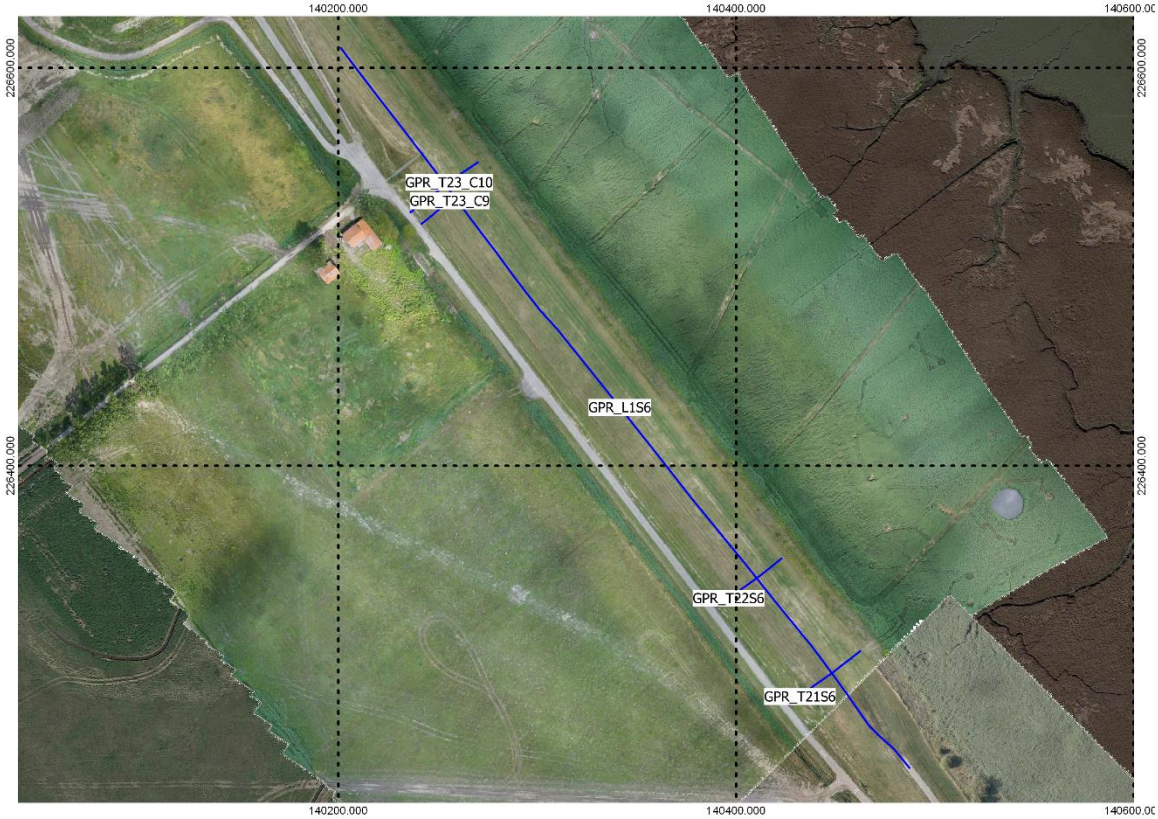

Figure 7: GPR profiles location of section 6

3.3 CPT and Permeafor

A cone penetration test (CPT) is a destructive geotechnical test where a cone attached to the end of a series of rods is pushed into the ground at a constant rate of 2 cm/s. In this case, electrical cones (CPTE) with a cross section of 10 cm² were used in combination with a 200 kN thrust machine. The resistance to penetration of the cone, q_c, and the friction of a the surface sleeve, f_s, are measured every 2cm. From these values the friction ratio R_f can be obtained ($Rf = f_s/q_c$). CPTs are well suited for soil profiling and classification. The cone resistance is typically large in sands and low in clays and peat, and the friction ratio (R_f) is low for sands and large for clays and very large for peat. Several correlations between CPT values and geotechnical parameters are available in literature. (a.o. Robertson, 1990 and Lunne et al. 1997).
In this report some soil classification figures are made, based on the Soil Behavior Type index as defined by Robertson (Robertson, 1990). These figures are referred to as 'Robertson figures'.

We tried to perform the Permeafor measurements where the geophysical profiles and CPTs were located. Unfortunately, for sections 10 and 11, matching the three methods was not possible, since no Permeafor was performed. Moreover, on some parts of sections 6, 10 and 11 under rainy conditions and relative wet surface, the Permeafor truck was too heavy to position the testing equipment on the crest. For the sections 2, 4, 6 and 11, the name of the drillings (CPT and Permeafor) with their GNSS coordinates in Lamberts 72 system are given in Table 3. The z coordinate represents the ground level in m TAW. Their locations are shown in Figure 8: Drillings (CPT and Permeafor) locations of section 4 .

Table 3: GNSS Coordinates in Lambert 72 system and z in m TAW of Permeafor (PK*), CPT (S*) and Shelby tube geotechnical testing by Cerema whose results are currently not available).

Section	Name	X L72 (m)	Y L72 (m)	Z (m)
4	S14	141029,37	225635,3	10,9
	S15	141008,32	225658,1	11,0
	S16	140985,27	225682,1	11,0
	S17	140966,56	225701,6	11,1
	S18	140945,61	225723,3	11,1
	S9BIS	141061,1	226417,7	10,9
	PK3_Sect4	140927,8	225741,6	9,1
	PK4_Sect4	140833,8	225841,4	6,8
	PK5_Sect4	140642,6	226041,0	4,6
	PK6_Sect4	140641,4	226042,0	4,4
	PK7_Sect4	140626,2	226027,8	-2,8
6	S1	140447,2	226294,6	11,7
	S2	140424,6	226323,5	11,8
	S3	140399,0	226355,3	12,0
	S4	140374,3	226385,9	11,9
	S5	140349,0	226417,7	11,8
	S6	140326,0	226447,4	12,0
	S7	140300,5	226478,3	11,9
	S8	140275,7	226510,7	11,8
	S9	140249,5	226545,0	11,8
	Shel1_Sect6	140388,9	226343,7	-2,8
	Shel2_Sect6	140241,4	226530,5	0,3
	PK8_Sect6	140464,0	226280,1	8,2
11	S178	139418,3	226569,5	4,7
	S179	139465,6	226597,2	4,8
	S180	139504,3	226619,6	4,7
	S181	139546,5	226644,2	4,7
	S182	139590,0	226669,4	4,7
	S183	139632,9	226694,1	4,7
	Shel3_Sect11	139589,8	226673,8	3,5
	PK9_Sect11	139576,7	226686,9	9,8

NB:The preliminary comparison between the CPT and the Permeafor measurements is presented in appendix. The curves seem to have a systematic deviation as a function of depth in the order of magnitude of 50 cm, which needs to be further explored.

Figure 8: Drillings (CPT and Permeafor) locations of section 4

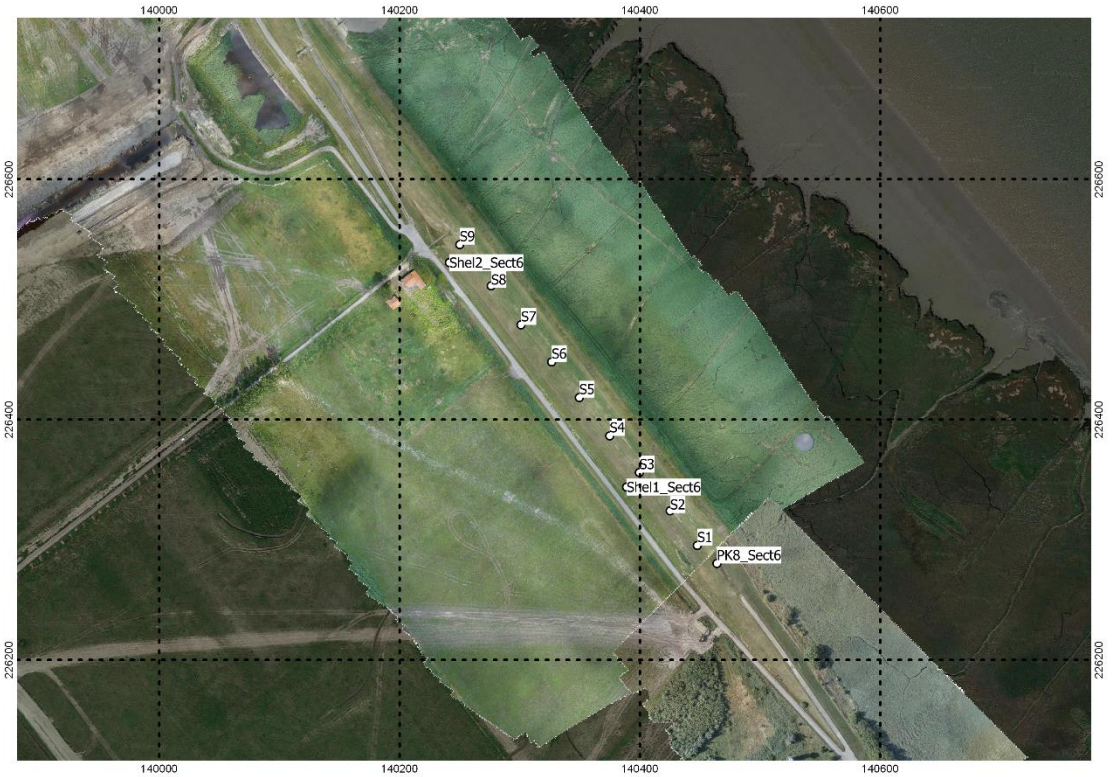

Figure 9: Drillings (CPT and Permeafor) locations of section 6

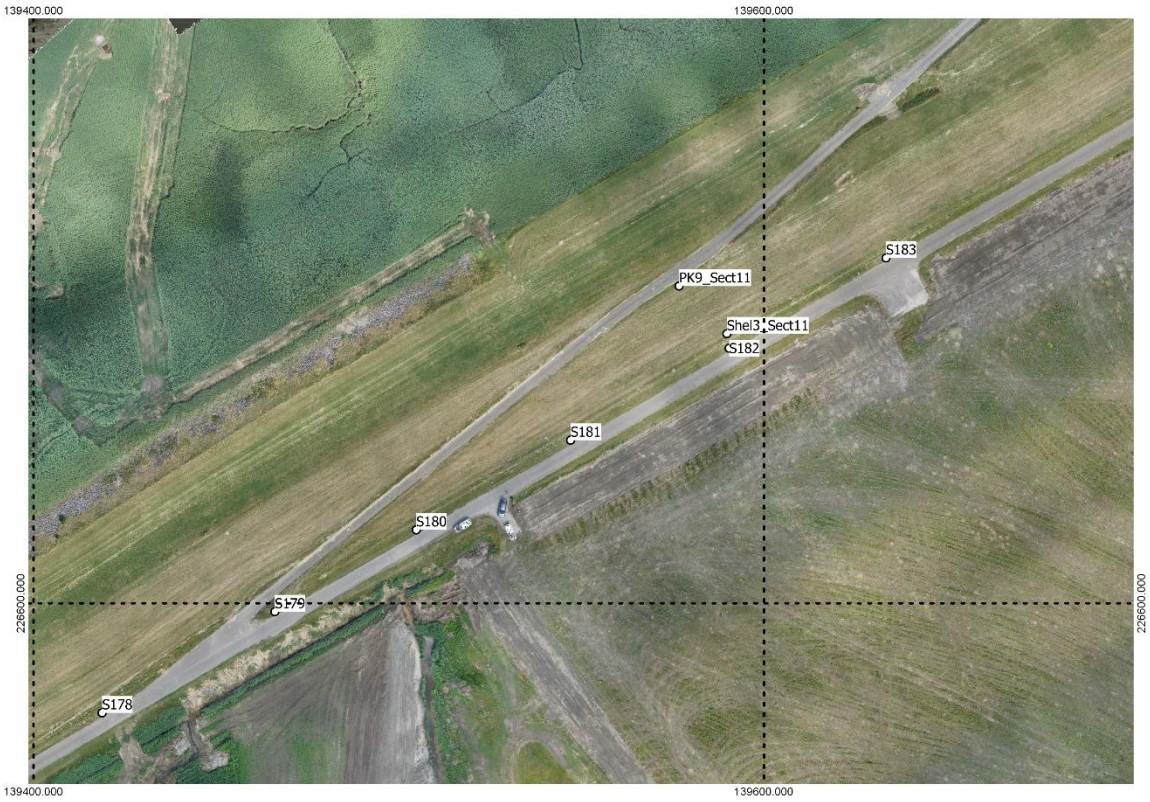

Figure 10: Drillings (CPT and Permeafor) locations of section 11

4 Main Results

4.1 Digital Elevation Model

The Digital Elevation Model was obtained thanks to photogrammetry. All images were formerly captured with drone by DMOW-ATO in June 2020. This DEM is used to properly show the geophysical measurements inside the 3D topography of the dike, rendering easier the visualization and the interpretation.

In Figure 11, a global view of the DEM is shown in Lambert 72 coordinates.

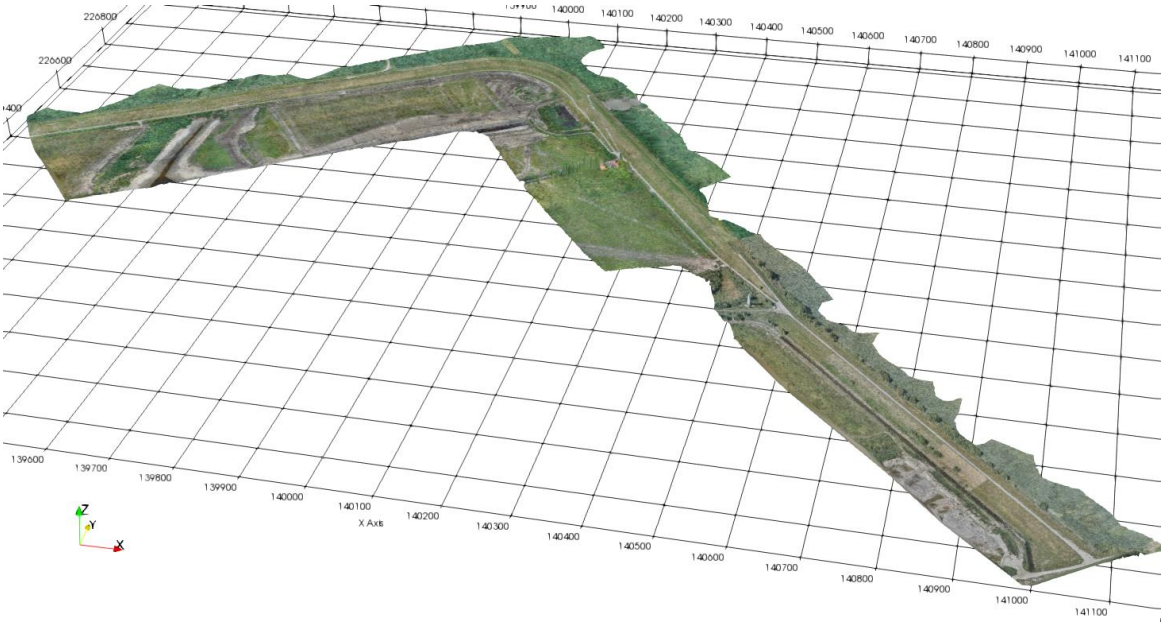

Figure 11: Global view of the DEM of the dike studied in LLHPP (coordinates in Lambert 72 system)

The UAV survey consisted of recording photographs at regular intervals according to a flight plan with a camera embedded on a drone. Thirty Ground Control Points (GCP's) visible on pictures are placed on the dike and geo-referenced thanks to a Global Navigation Satellite System (GNSS). The drone survey in the Dutch sections 6, 10 and 11 was performed at 86 m height and leads to a strip of about 1800 m length and 390 m width while the Belgium sections 2 and 4 were obtained with a drone flight at 54 m height, leading to a strip of about 1950 m length and 250 m width. In Figure 11, only the section 4 is shown in the Belgian part.

In the Dutch sections, 1455 images were captured and the calculated error is about 3 cm, 3.7 cm and 2.7 cm in the x, y and z directions, respectively (total error of 5.5 cm, projection error of 0.415 px). In the Belgium sections, 5800 images were captured and the error is about 0.9 cm, 1 cm and 1.1 cm in the x, y, and z directions, respectively (total error of 1.7 cm, projection error of 0.361 px).

4.2 Electrical Resistivity Tomography, Ground Penetrating Radar and Geotechnical Testing

4.2.1 Section 4

4.2.1.1 Whole overview of geophysical results in section 4

In Figure 12, an overview shows the 2 longitudinal profiles (one on the crest, left to the road border and the other at the toe) and the 3 transverse profiles carried out on section 4.

The ERT profile carried out on section 4 on the crest shows:

- a shallow surface quite resistive (100 to 200 Ω.m), corresponding to the road materials (of about 1 m thick) layer and to the top clayey layer depicted by the geotechnical analysis;
- followed by a more resistive layer (sometimes more than 1000 Ω.m) till 10 m depth corresponding to the dike core, mainly composed of sandy materials;
- a very conductive layer (few Ω.m) over 10 m depth, corresponding to the bottom of the dike and that may be the natural subsoil of LLHPP. In this zone, the conductivity is also strongly influenced by the ground water. As can be seen in Figure 13, the ground water level in the dike was at about 2.5 m TAW in October 2020, which means it is situated at a depth of approximately 8.5 m from the dike crest. Since the Scheldt water is salt water, it can be supposed that the water in the dike is brackish water, which has a strong influence on the electrical resistivity.

The ERT profile at the toe contains a shallow layer (about 3m thick) of low resistivity (around 20 Ω.m), followed by the natural subsoil of the LLHPP, where the resistivity is low and similar to the deeper layer of the ERT longitudinal profile.

The 3 transverse ERT profiles offer a visualization of the materials distribution across de dike. Main layers and resistivity are correlated to the longitudinal profiles resistivity. The natural earth surface layer is clearly delimited as a shallow surface of about 50 Ω.m.

Nevertheless, the resistivity maps of transverse profiles are slightly higher than the longitudinal ones and the delimitation between two layers (for instance, the core and natural subsoil at the bottom of the dike) don't show the same depth between a transverse and a longitudinal profile. We suppose that this effect can be removed if the inversion of ERT data is performed considering the 3D topography of the dike.

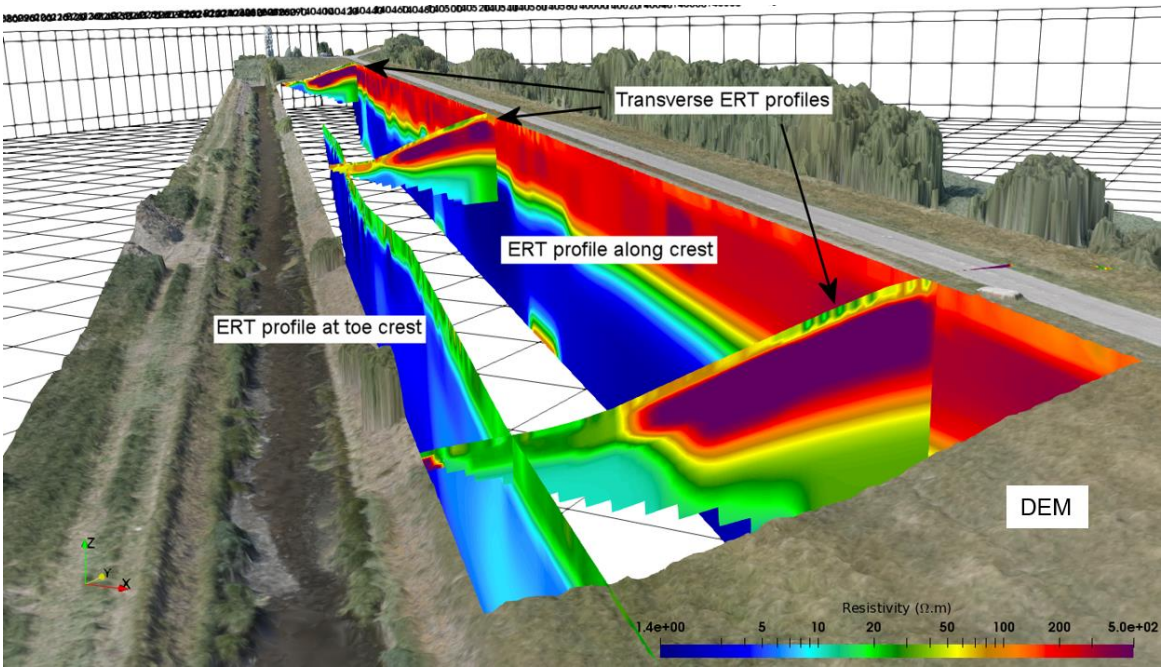

Figure 12: Global view of the 2 ERT longitudinal profiles on the crest ERT_L1_S4 and the toe ERT_L2_S4 of the dike and the 3 ERT transverse profiles, ERT_T10_S4, ERT_T11_S4 and ERT_T12_S4 included in the DEM, section 4.

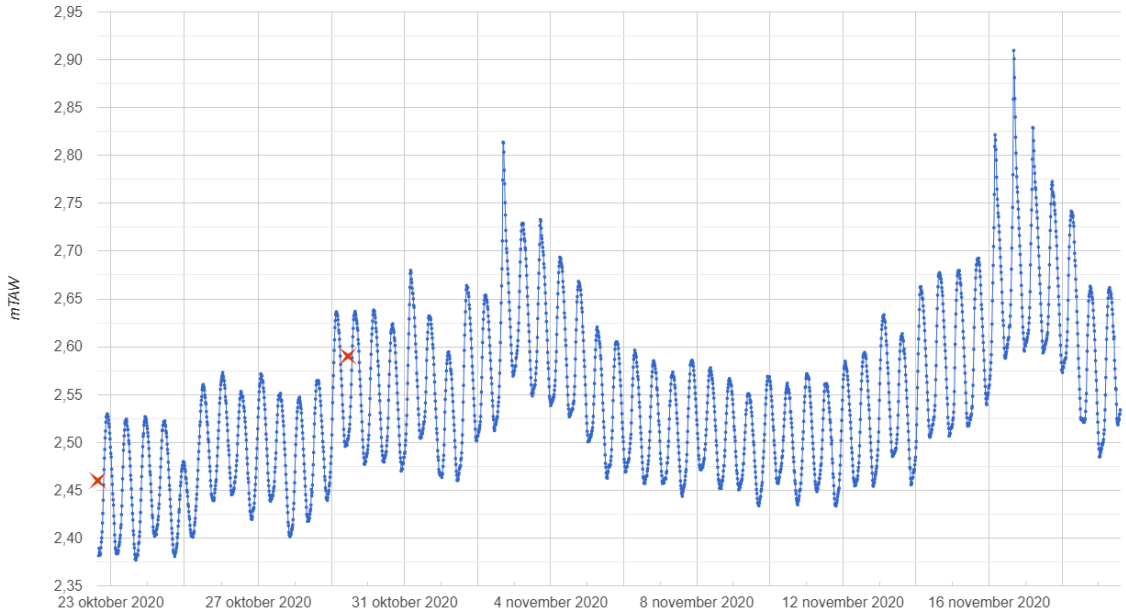

Figure 13: Ground water measurement in dike: monitoring well Pb18a in section 4 for time interval October-November 2020 (DMOW – Geotechnics division).

Figure 14 and Figure 15 show a focus on the transverse profile ERT_T10_S4 and the corresponding GPR profile GPR_T10_S4. ERT offers a better rendering of the material distribution in the dike: the core appears as a resistive layer and the natural soil seems to begin at approximately 6 m depth from the crests. This depth is lower than the depth showed on the longitudinal profile. Indeed, the transverse profiles have a lower depth of investigation than the longitudinal ones and consequently, the level of confidence in this outcome is low. The surface earth material of about 0.5 to 1 m depth corresponds to the shallower layer (resistivity from 20 to 50 Ω.m). The road structure is clearly identified (anomaly A1 in Figure 14). The river bank of the dike (second anomaly blue-encircled in

this figure) seems to contain a more resistive part (more visible in the top Figure 16) that may correspond to a two-step construction phase for this side or to the use of two different materials.

The GPR profile globally presents a low contrast image except (i) at the crest where a layered media corresponds to the road structure and its transition to the slopes and (ii) at the bottom of the left flank where a layered structure can correspond to the implementation of materials. The top layer was identified as clayey materials thanks to the geotechnical analysis in the laboratory. Unlike what could have been foreseen, the GPR does apply in this LLHPP case. First, the main wavelength[1] into the subsoil can be estimated at about 0.5 m. It means that despite the near surface materials have a resistivity less than 100 Ω.m, we see that enough electromagnetic energy can pass through this layer and allow to produce relevant GPR images of the dike. This is true for the entire survey performed on the LLHPP.

In this work, we didn't perform an analysis of all GPR signals since many anomalies are present.

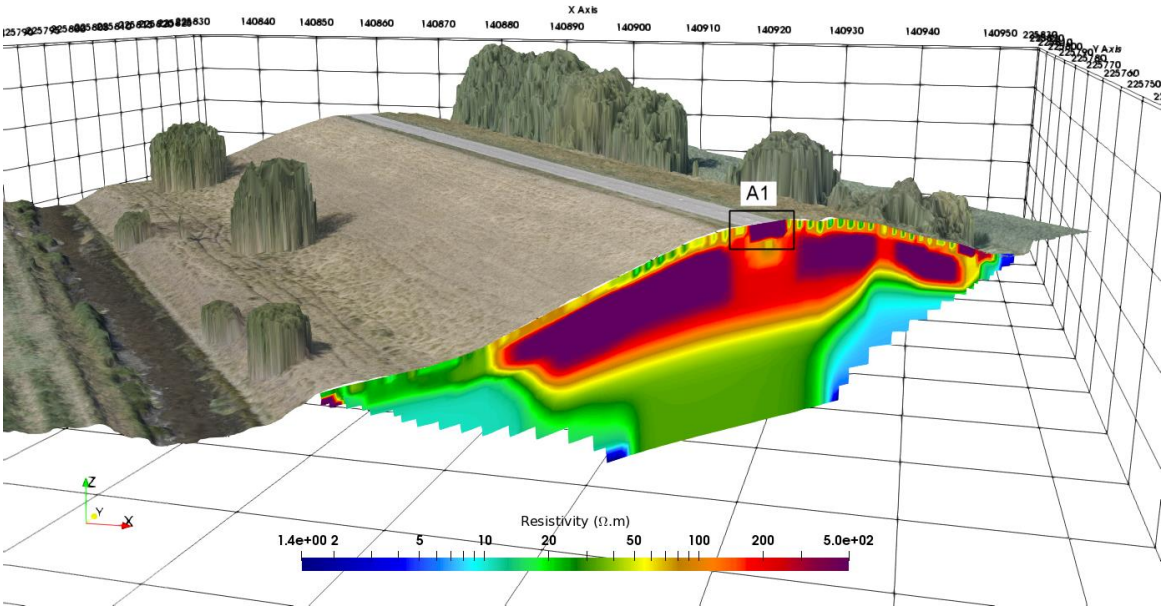

Figure 14: Only ERT transverse profile ERT_10_S4, section 4. Anomaly A1 is the road structure.

[1] *At 200 MHz, considering a real permittivity of 9 for the top layer, the wavelength in the materials is about 0.5 m.*

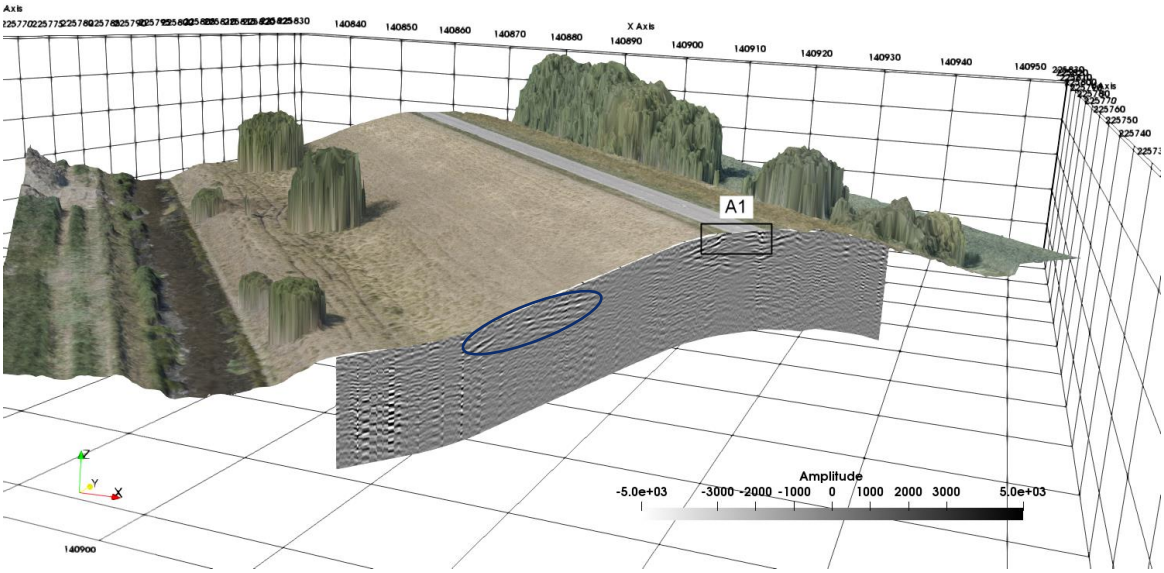

Figure 15: Same section 4 as the previous figure, with the transverse GPR profile GPR_T10S4. Anomaly A1 is the road structure. The other anomaly at the bottom of the slope shows a layered media.

4.2.1.2 Comparison between transverse ERT, GPR and CPT results

The interpretation of the ERT and GPR measurements can be enhanced, using the CPT and drilling results.

The correlation with CPT S18 can enrich the interpretation (see Figure 16): the *qc* value is small in the top layer and gradually gets larger at a depth between 0.5 and 1 m, where the ERT shows a transition between a clayey top layer and a sand core, and where the GPR shows a layered shallow structure corresponding to the road platform. At 8 m depth the *qc* value indicates a transition between sandy materials (blue color in the CPT interpretation, red one on ERT map) and a more clayey layer. Here, the CPT facilitates a better interpretation of the ERT results. It needs to be mentioned that the color maps, generated based on the correlations by Robertson (Robertson, 1990) do not always perfectly represent the *in situ* soil name. For instance, the 'sensitive, fine grained' soil can be identified as a sandy silt/clay layer, based on the drillings and laboratory tests. Another example is that the peat layers should be slightly thicker than indicated in the color pictures, as is the case for S14, S15 and S16. For this reason a manual soil layer composition has been made for a reference CPT, S18, as is shown in

Figure 17. The corresponding geotechnical parameters are given in Table 4.

On the Dutch part, generally a clear clayey top layer of approximately 1 m thickness can be noticed in the CPTs *(e.g. GEO-18/110 S1 & S3, see CPT annex)* and drillings *(e.g. GEO-18/111 B1A & B3A, see report on lab tests by De Backer & D'heer)*. In contrast to the Dutch part, the results from the CPTs and drillings on the Belgian part reveal a less clayey and less thick top layer. A rather small increase in Rf is found in CPT S18 (

Figure 17) in the top layer and drilling B18B (Figure 16) even indicates a sandy top layer. On the other hand, the laboratory tests on grain size distribution from the manually taken samples of the top layer in this area *(b4-IV.4 en b8-IV.2)* indicate that this layer is a sandy clay layer (25-36% clay; 34-40% silt and 24-41% sand). In conclusion, a top layer above the sand core is also noticed on the Belgian side of the dike, consisting of sand, silt and clayey material in varying quantities and with a thickness of generally less than 1 m.

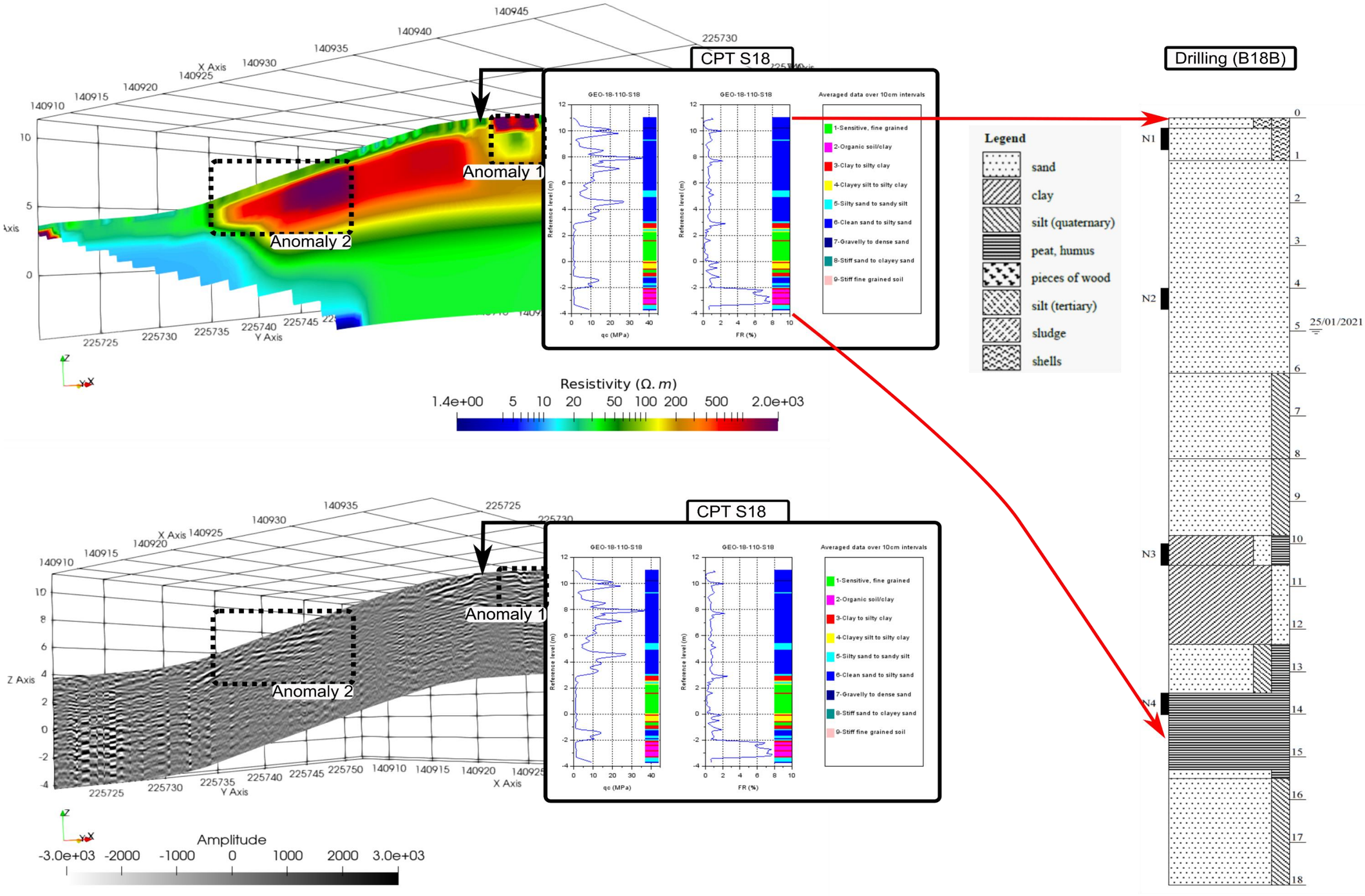

Figure 16: Comparison of CPT S18 soil layer interpretation based on Robertson SBT for ERT_T10_S4 profile (top) and GPR_T10_S4 profile (bottom)

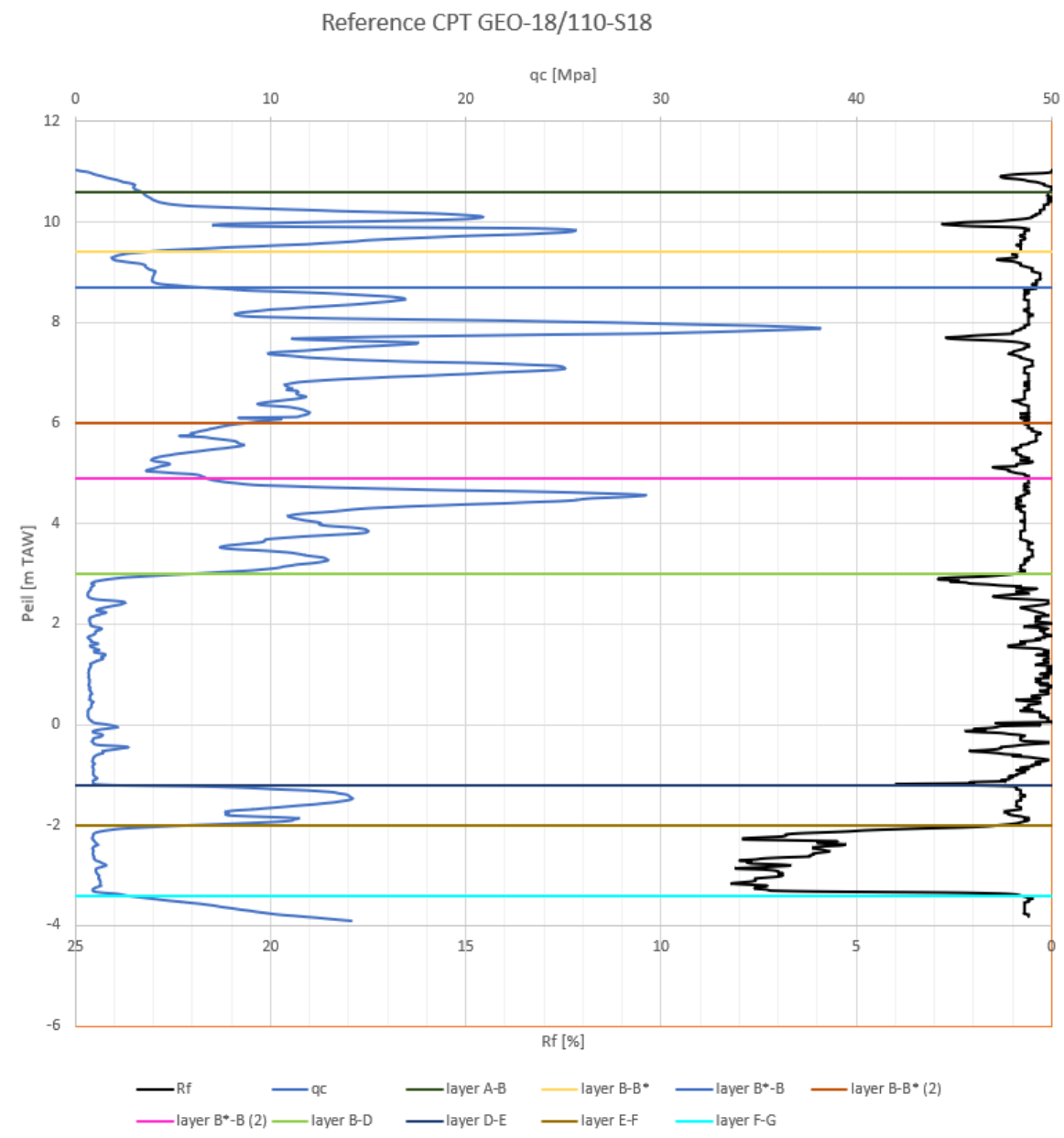

Figure 17: Soil layers at S18

The name of the soil type, the division between backfill soil (A), quaternary layers (Q) and tertiary layers (T), as well as an estimation of the geotechnical characteristics are given in Layer structure and soil characteristics based on CPT GEO-18/110 – S18, section 4 (A= backfill soil, Q=Quaternary, T= tertiary). The geotechnical characteristics are based on the Eurocode 7 values (NEN 6740 table (Nl) - NAD table from EC7 (BE)).

When these values are compared to the results of the triaxial tests that were carried out in the lab on undisturbed samples for this project, it can be concluded that the values mentioned in these tables are conservative.
The results of the lab tests, can be found in the report on the drillings and lab tests GEO-18/111 ((Griet De Backer and Stefanie D'heer, 2021).

Table 4: Layer structure and soil characteristics based on CPT GEO-18/110 – S18, section 4 (A= backfill soil, Q=Quaternary, T= tertiary)

Layer [-]	**Upper level** [m TAW]	**Description** [-]	γ_d [kN/m^3]	γ_n [kN/m^3]	ϕ' [°]	c' [kN/m^2]	**A/Q/T**
A	11,09	moderately firm sandy, silty clay/ sandy, clayey silt/ clayey, silty sand	18	18	25	2	A
B	10,59	densely packed clayey/silty sand	18	20	30	0	A
B'	9,4	moderately packed clayey/silty sand	17	19	27	0	A
B	8,7	densely packed clayey/silty sand	18	20	30	0	A
B'	6	moderately packed clayey/silty sand	17	19	27	0	A
B	4,9	densely packed clayey/silty sand	18	20	30	0	A
D	3	slightly firm to moderately firm sandy clay	18	18	25	2	Q
E	-1,2	densely packed sand	18	20	32	0	Q
F	-2	solid peat	14	14	15	10	Q
G	-3,42	densely to very densely packed sand (see also S17)	18	20	32	0	Q

4.2.1.3 *Comparison between transverse ERT_L1_S4 profiles with CPT 14 to CPT 18*

In the Figure 18, we compared the ERT_L1_S4 profile with CPT S14 to S18. The Permeafor locations are also indicated but not interpreted yet. From the Figure 19 to the Figure 23, the CPTs are compared individually with the local ERT profiles. Globally, in all these figures, the depth resolution of the CPT curves is thinner than the ERT data. CPT information can precisely depict the subsoil layering of the order of 5 cm while ERT resolution in function of depth is of the order of 1 meter. Moreover, the transition between layers in ERT data is smooth and the depth of an interface between two layers of different materials can not be assessed precisely.

The ERT results globally depict:

- the silty sand and sandy silt top layer (around 200 Ω.m) at the surface to about 1 to 1.5 m depth (i.e., from level 10.7 m to 9.7-9.2 m TAW);
- Followed by the dense and clean sand formation (around 2000 Ω.m from level 9.5 m to 5 m TAW), The small intermediate clayey layer which is visible in CPT S14 at 5 m TAW, is not visible in the ERT images;

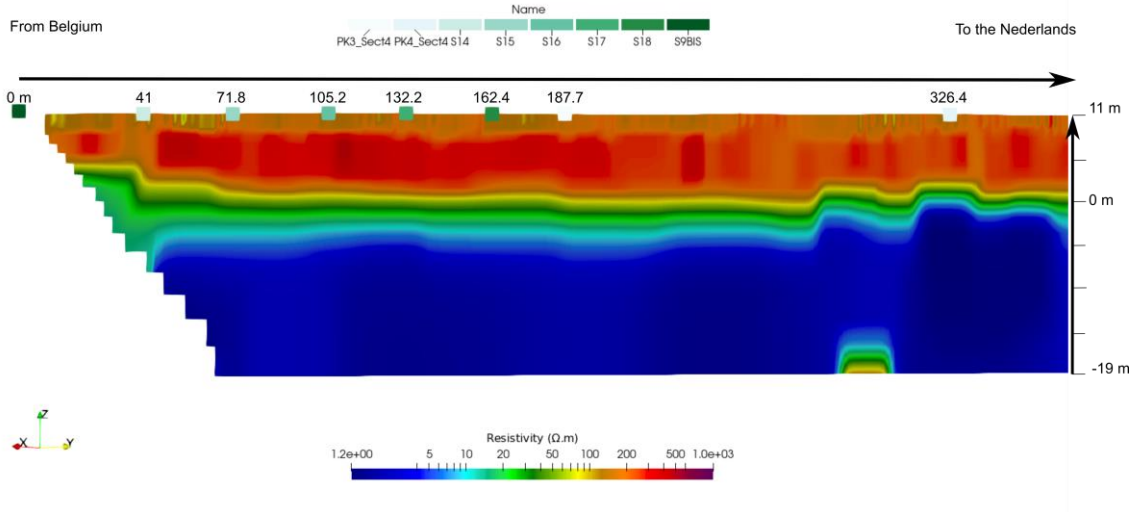

Figure 18: Section 4, Belgium part, with the ERT_L1_S4 profile and the CPTs and Permeafor locations. Only S14 to S18 are compared with ERT measurements.

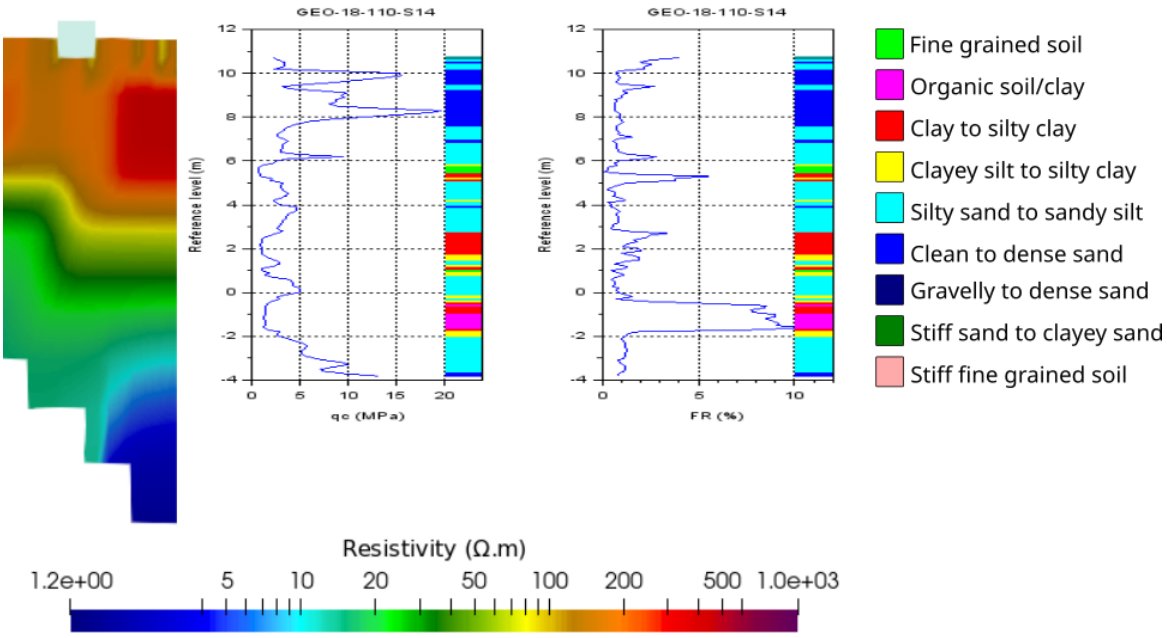

Figure 19: Resistivity compared with qc factor and friction ratio at CPT S14 location

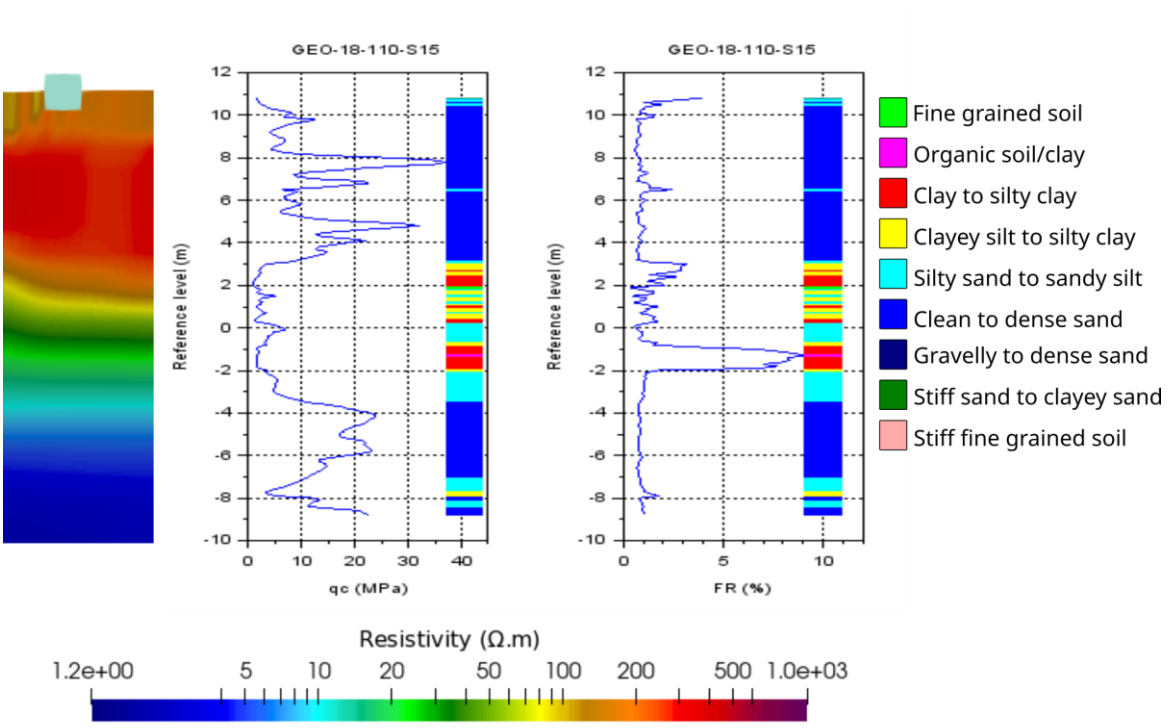

Figure 20: Resistivity of ERT_L1_S4 profile compared with qc factor and friction ratio at CPT S15 location

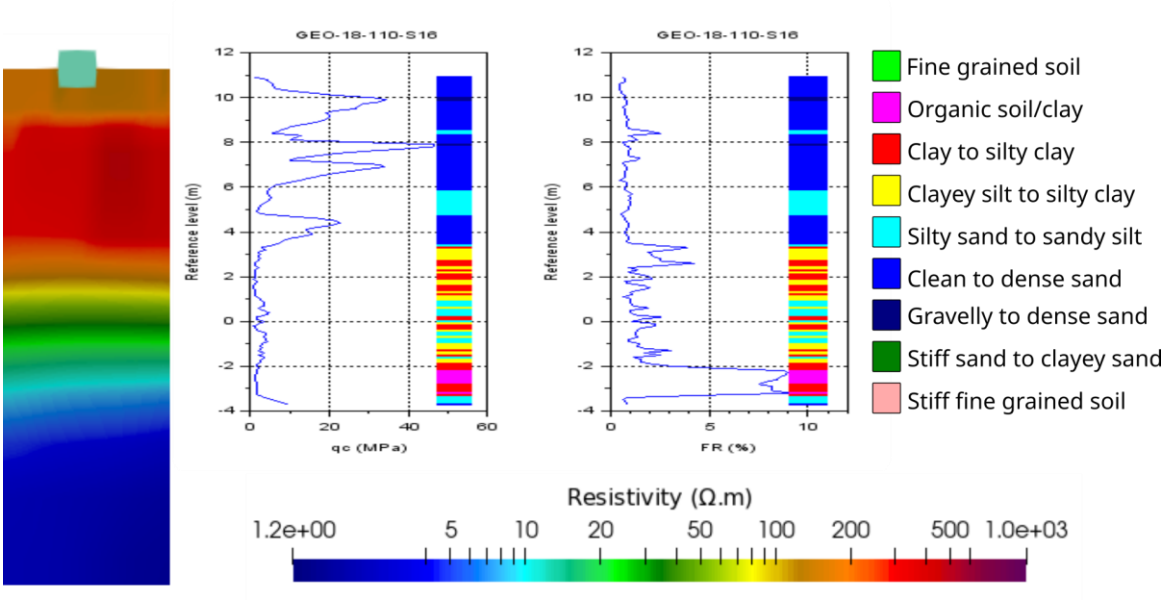

Figure 21: Resistivity of ERT_L1_S4 profile compared with qc factor and friction ratio at CPT S16 location

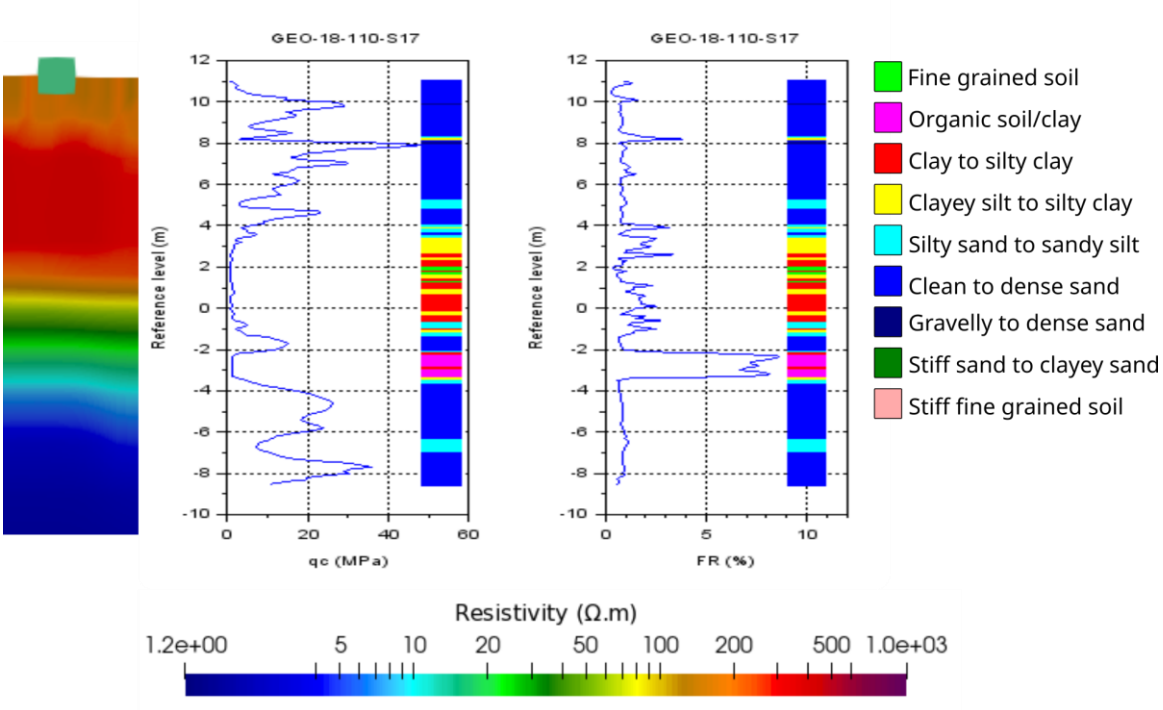

Figure 22: Resistivity of ERT_L1_S4 profile compared with qc factor and friction ratio at CPT S17 location

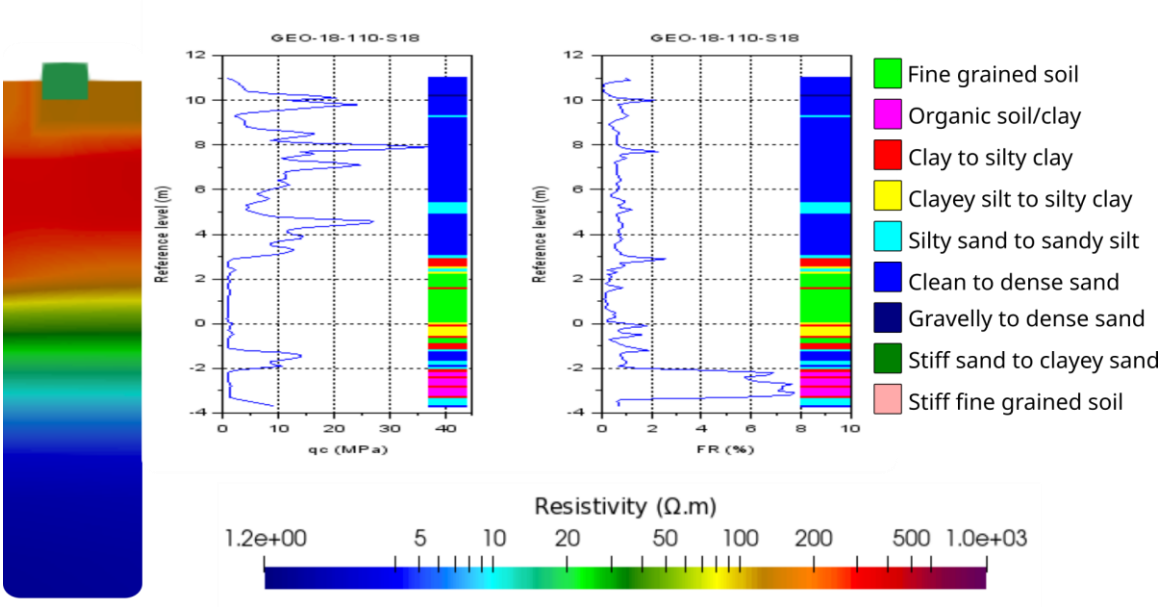

Figure 23: Resistivity of ERT_L1_S4 profile compared with qc factor and friction ratio at CPT S18 location

4.2.2 Section 6, South-East

4.2.2.1 Overview of section 6, South-East ERT

Five ERT profiles were performed on the beginning of the section 6 (see Figure 24).

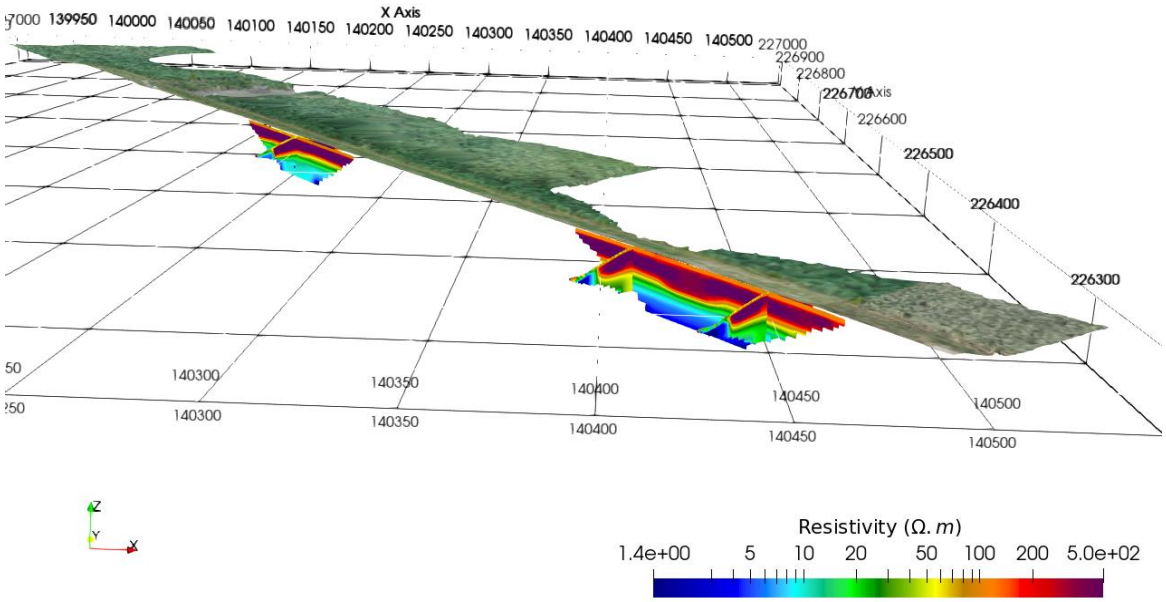

Figure 24: Global view of ERT profiles on section 6. Section 6 North at the left, section 6 South at the right.

4.2.2.2 ERT and GPR measurements on section 6, South-East

Figure 25 focuses on the South-East of the section 6 and shows the longitudinal ERT profile ERT_L1_S6 with the 2 ERT transverse profiles ERT_T21_S6 and ERT_T22_S6. A similar structure is observed between the Belgian section 4 and the Dutch section 6. Nevertheless, core materials are slightly less resistive, particularly in the river side of the dike, as depicted in Figure 25.

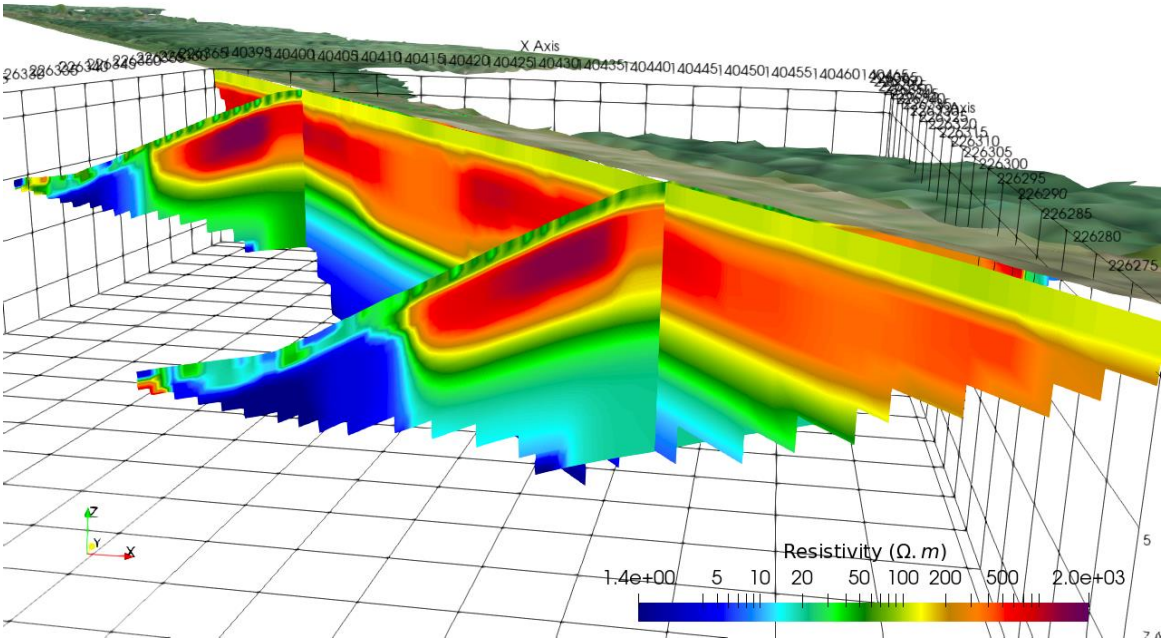

Figure 25: South of the section 6 with the longitudinal ERT_L1_S6 profile and the transverse ERT_T21_S6 (left) and ERT_T22_S6 (right) profiles

In Figure 26 and Figure 27, the longitudinal GPR profile GPR_L1_S6 with the 2 transverse profiles GPR_T21_S6 (right in the figure) and GPR_T22_S6 (left of the figure) are shown. The earth shallow layer is clearly visible on both transverse profiles. Some local anomalies are present in the longitudinal profile. Information is limited as far as concerned the rest of the 3 profiles, deserving a deeper analysis, complementary measurements with other methods or drillings and correlation with dike history data.

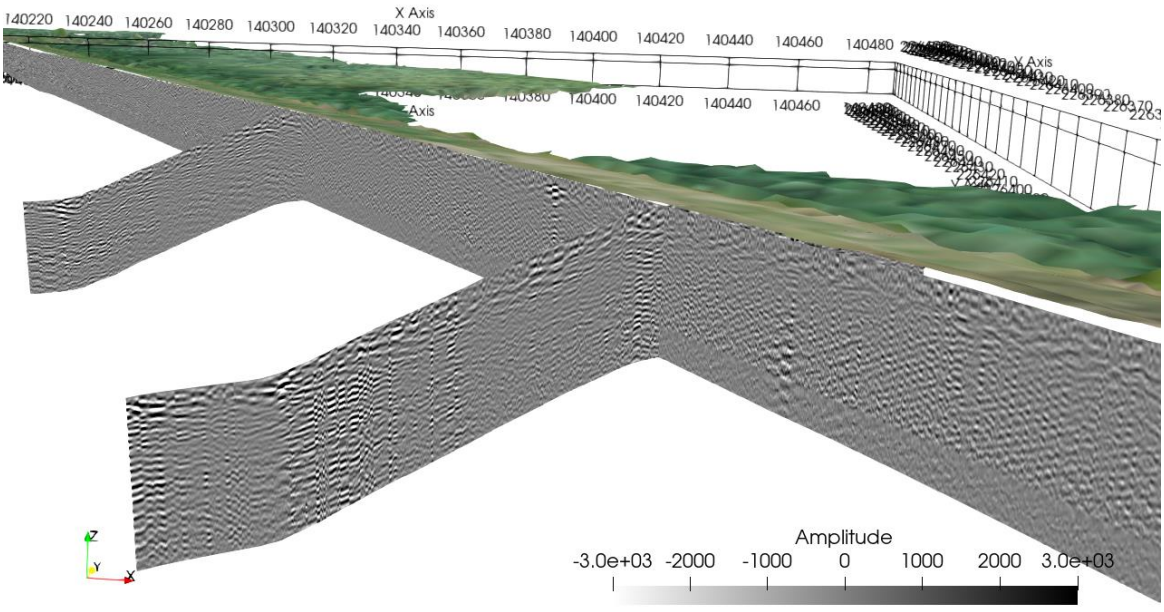

Figure 26: South of the section 6, longitudinal GPR profile GPR_L1_S6 with the 2 transverse profiles GPR_T21_S6 (right in the figure) and GPR_T22_S6 (left of the figure).

Figure 27 and Figure 28 focus on transverse ERT and GPR profiles. The clayey top layer is well depicted by both methods. Here, there is no road structure and surprisingly, the materials under the crest on the ERT profiles appear less resistive while the GPR dielectric contrast is visible as deep

as in the Belgian part. It can be a 3D effect or may be the materials differ from under the slopes to under the crest of the dike.

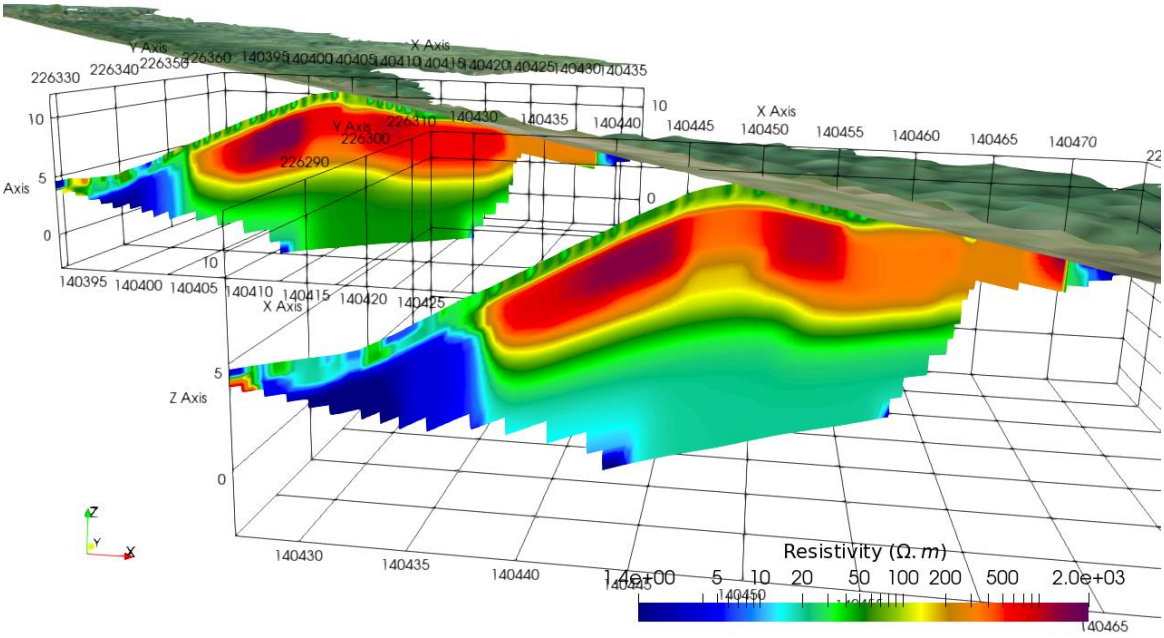

Figure 27: South of the section 6 with the transverse ERT_T21_S6 (left) and ERT_T22_S6 (right) profiles

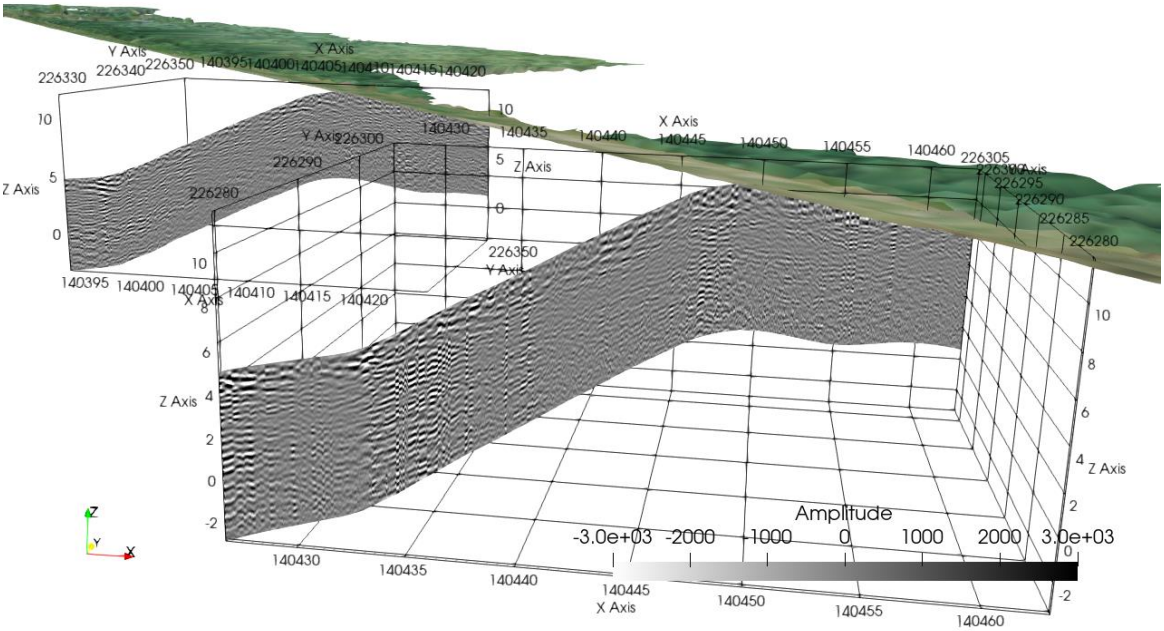

Figure 28: South of the section 6, CPR transverse profiles GPR_T21_S6 and GPR_T22_S6

4.2.2.3 Comparison between transverse ERT and GPR profiles with CPTs and Permeafor

In the Figure 29, a shallow layer of about 1 m thick corresponds to the clay top layer, followed by a sandy layer till 3 m depth, alternating silty/clayey layers from 3 to 5 m depth, and again a sand layer from 5 to 9 m depth, all corresponding to the dike core. From a depth of 9 m, a natural clay layer, most likely sedimentary clay, is encountered.

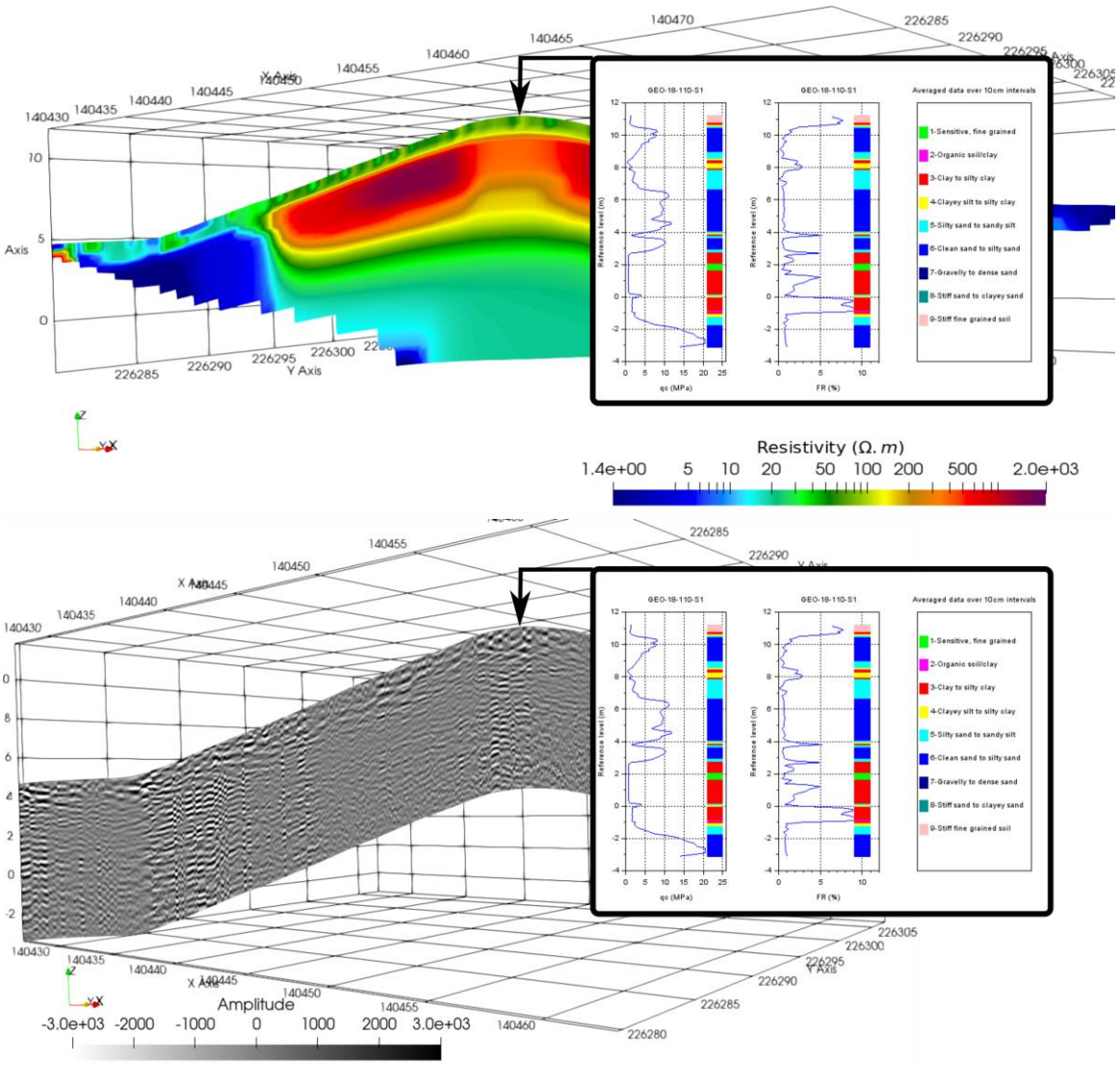

Figure 29: Comparison of CPT S1 interpretation with ERT_T21_S6 profile (top) and GPR_T21_S6 profile (bottom)

A ground layer structure has been made for GEO-18/110– S3 corresponding to section 6 (Figure 36).

The name of the soil type, the division between backfill soil (A), quaternary layers (Q) and tertiary layers (T), as well as an estimation of the geotechnical characteristics are given in Table 5. As for S18 of section 4, the geotechnical characteristics are based on the Eurocode 7 values (NEN 6740 table (Nl) - NAD table from EC7 (BE)), and are generally conservative compared to the results from the laboratory test.

The results of the lab tests, can be found in the report on the drillings and lab tests GEO-18/111. (De Backer & D' Heer, 2022)

Table 5: Layer structure and soil characteristics based on CPT GEO-18/110 – S3, section 6

Layer [-]	Upper level [m TAW]	Description [-]	γ_d [kN/m^3]	γ_n [kN/m^3]	ϕ' [°]	c' [kN/m^2]	A/Q/T
A	11,95	moderately firm sandy clay	17	17	25	2	A
B	10,95	(clayey/silty) loosely packed sand, with thin clay-silt layer around 10 m TAW	16	18	25	0	A
C	8	Very densely packed sand	18	20	35	0	A
D	3,2	slightly firm to moderately firm sandy silt, with sand lens around 2 m TAW	17	17	25	2	Q
F	0,2	solid peat	14	14	15	10	Q
G	-0,8	densely to very densely packed sand	18	20	32	0	Q

4.2.2.4 Comparison between CPTs S1, S2 and S3 with ERT_L1_S6

In the Figure 30, we compared the ERT_L1_S6 profile with CPT S1 to S3. The Permeafor PK8_Sect6 location is also indicated but not interpreted yet (see appendix section). From the Figure 31 to the Figure 33, the CPTs are compared individually with the local ERT profiles. Similarly to section 4, the depth resolution of the CPT curves is thinner than the ERT data. CPT information can precisely depict the subsoil layering of the order of 5 cm while ERT resolution in function of depth is of the order of 1 meter. Moreover, the transition between layers in ERT data is smooth and the depth of an interface between two layers of different materials can not be assessed precisely.

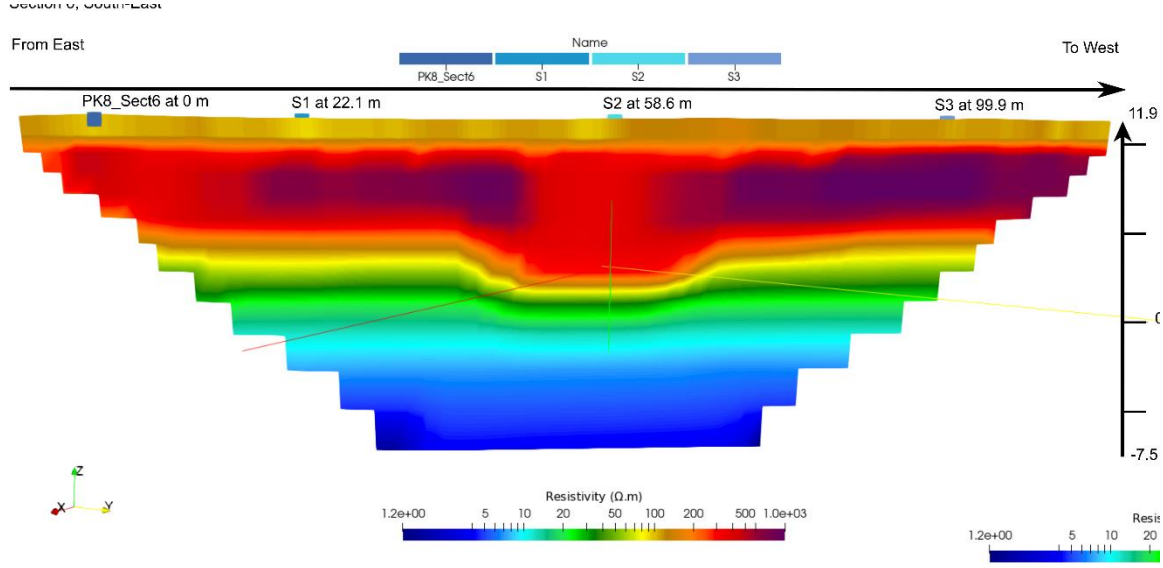

Figure 30: Section 6, South-East, with the ERT_L1_S6 profile and the S1 to S3 CPTs.locations (at the top ERT image) and PK8_sect6

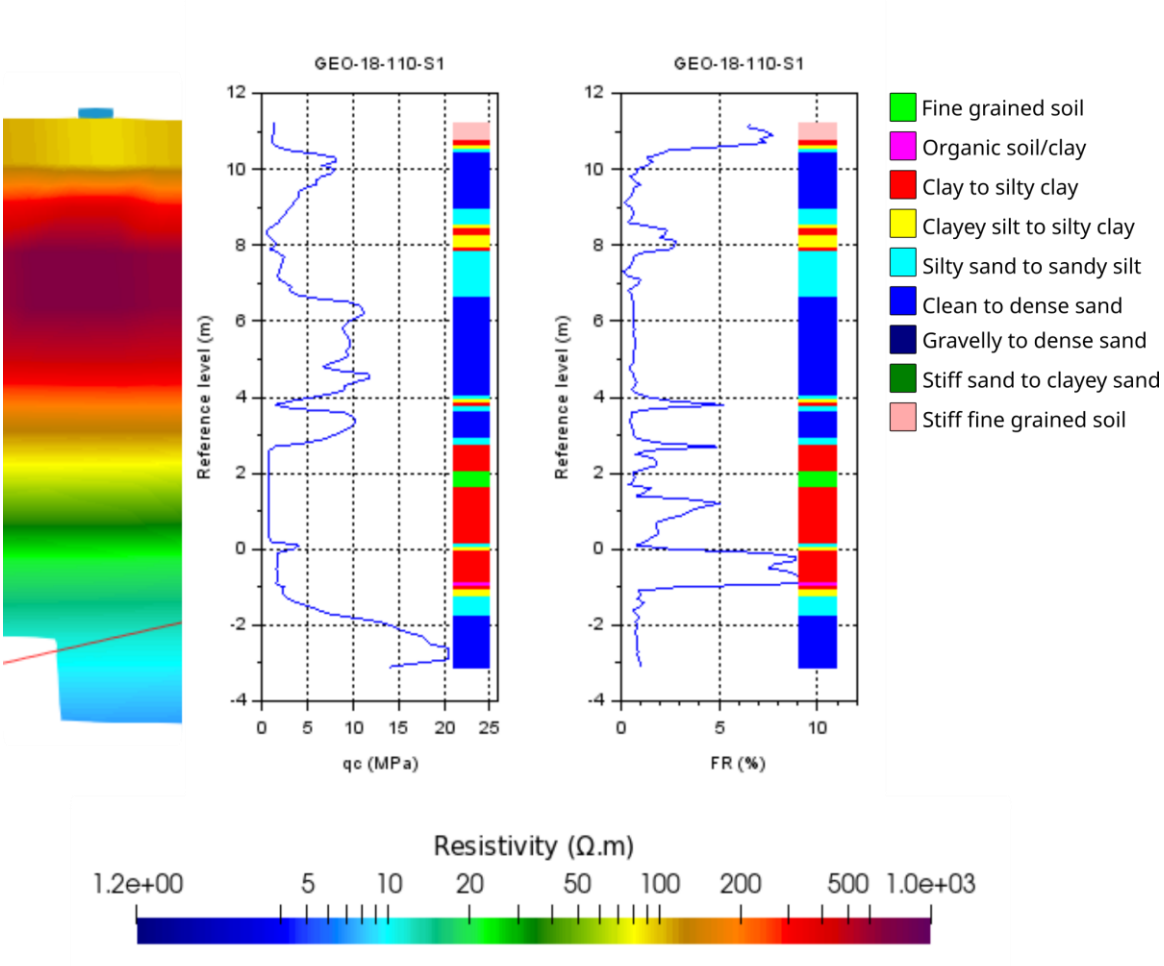

Figure 31: Resistivity of ERT_L1_S6 profile compared with q_c and R_f at CPT S1 location

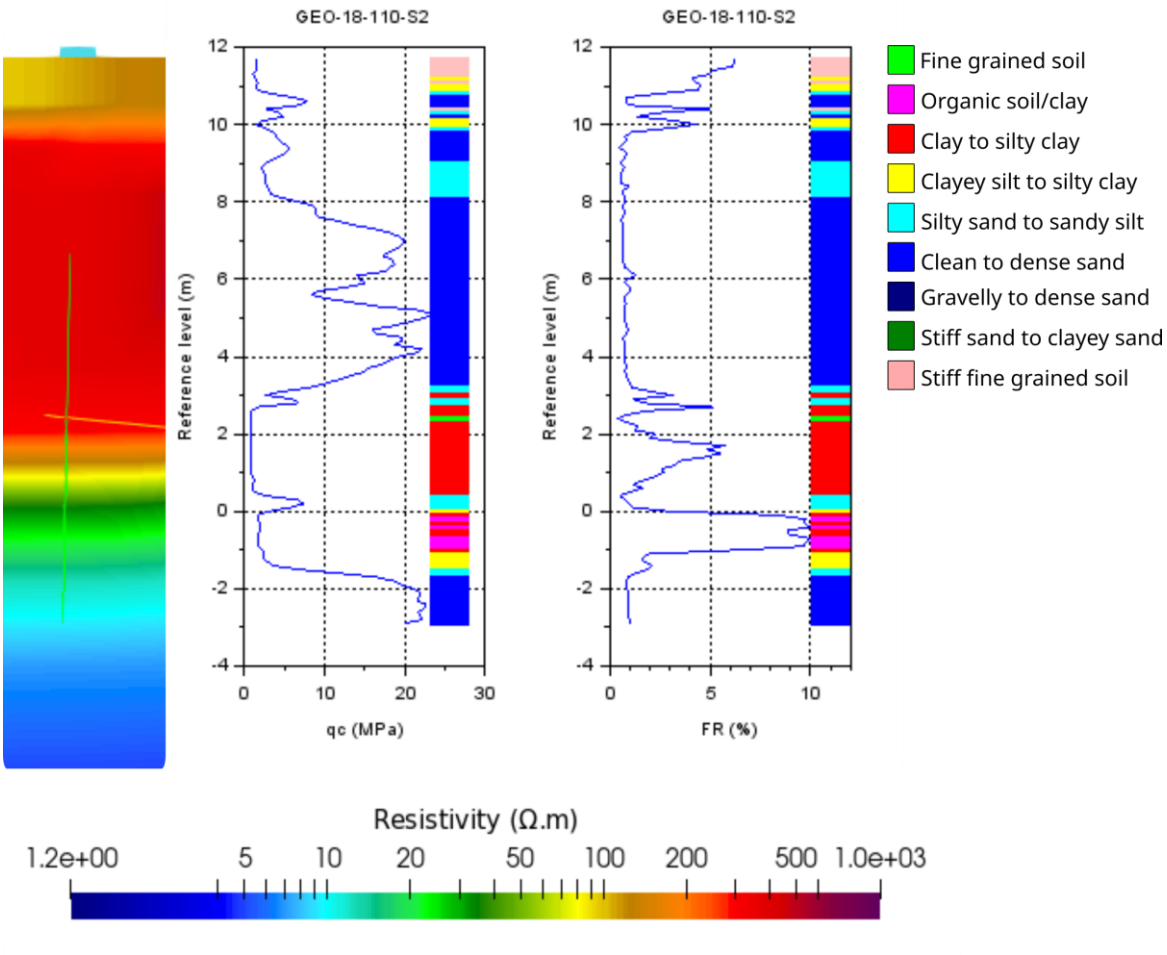

Figure 32: Resistivity of ERT_L1_S6 profile compared with q_c and R_f friction ratio at CPT S2 location

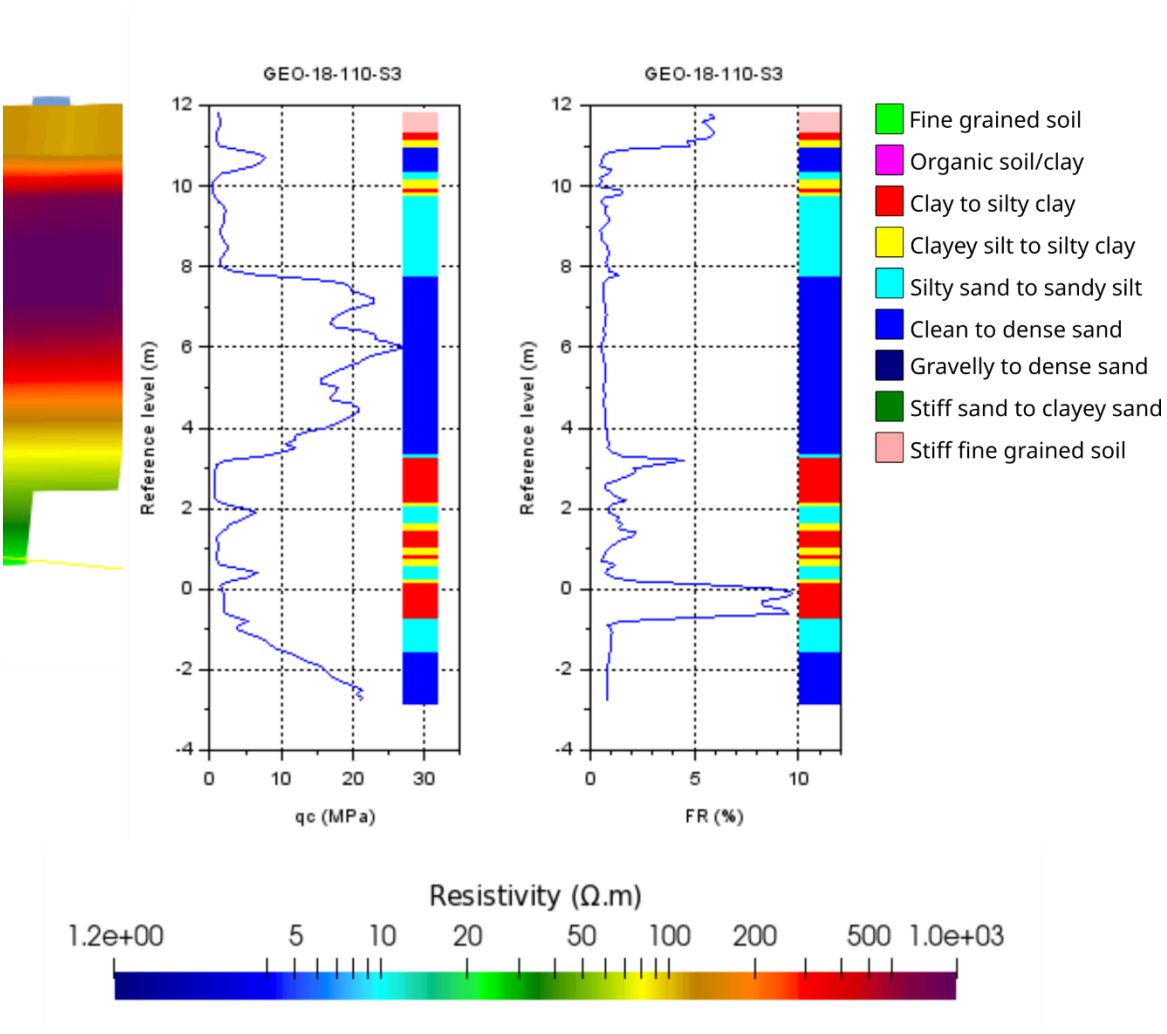

Figure 33: Resistivity of ERT_L1_S6 profile compared with with q_c and R_f at CPT S3 location

Note that in Figure 33 - S3, the soil characterization of Robertson shows between 0 and -1 m TAW 'clay to silty clay' instead of a peat layer. Based on the drilling B3A and lab tests, it is known that this layer has an organic content of 77.5 %, and consequently it is a peat layer without any doubt. For this reason, a manual soil layer composition has been made for CPT S3, as is shown in Figure 34. The layer names correspond to those mentioned in Table 5.

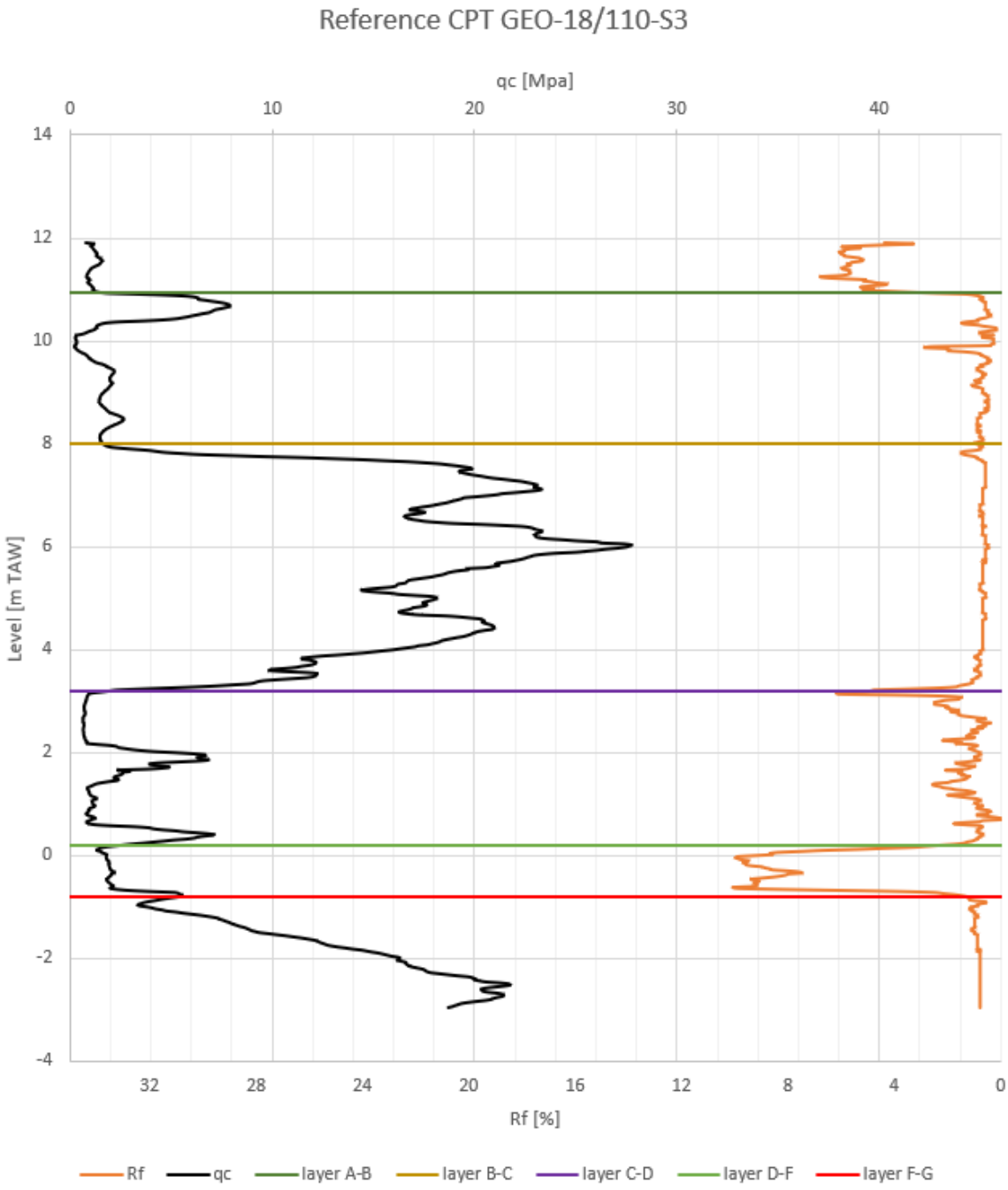

Figure 34: Soil layers at S3

4.2.3 Section 6, North-West (towards the Netherlands)

4.2.3.1 Overview of Section 6, North-West

The longitudinal ERT profile ERT_L2_S6, the transverse ERT profile ERT_T23_S6 and the corresponding longitudinal GPR profile GPR_L1_S6 and transverse GPR profile GPR_T23_S6 are shown in Figure 35 and Figure 36, respectively.

Compared to Figure 25 and Figure 27, the resistivity corresponding to the dike core is generally higher, but the global dike materials distribution remains identical. Both ERT and GPR profiles show a clayey top layer of 0.5 to 1 m thick. As well as for the sections 4 and 6-South, longitudinal ERT results give a 3 layer materials distribution (clayey top layer (0 to 0.5-1 m depth), dike core (1 m to 6 to 9 m depth) and natural clay layer (starting at around 9 m depth). The transverse profile shows (i) a homogeneous core, with clear transition from resistive core to conductive materials (clay) at the land slope toe and (ii) perhaps a 2 phase work at the river bank toe. GPR results are more difficult to interpret but the clayey top layer can be clearly delimited.

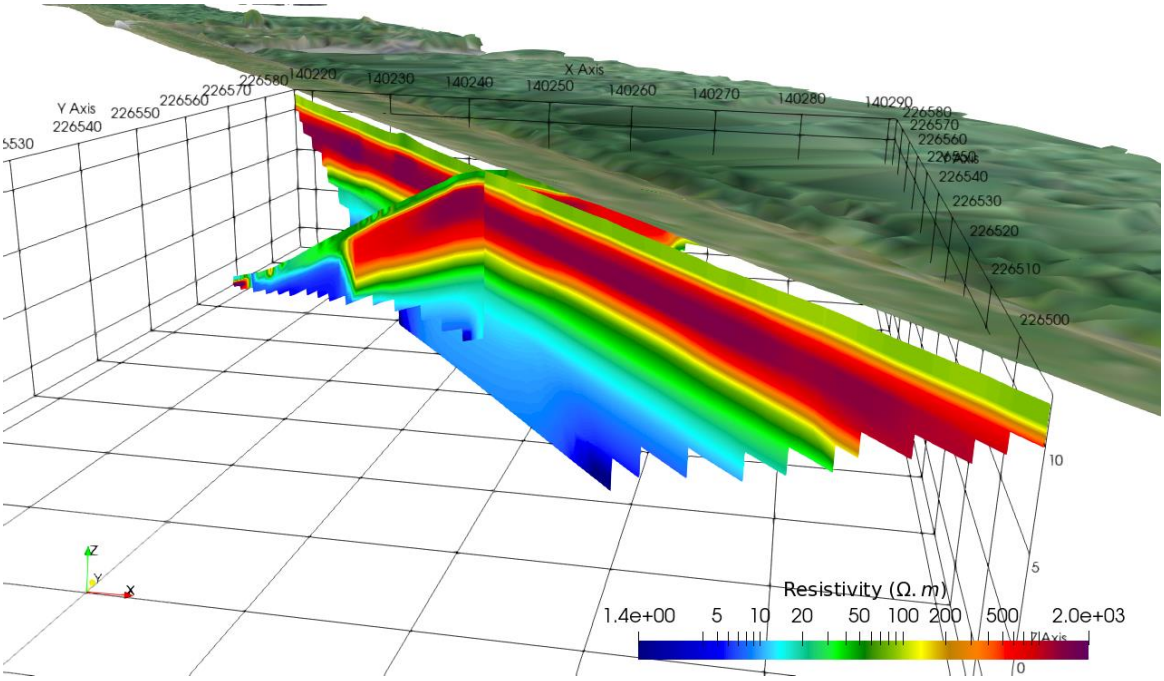

Figure 35: North of the section 6 with the longitudinal ERT_L2_S6 profile and the transverse ERT_T23_S6 profile

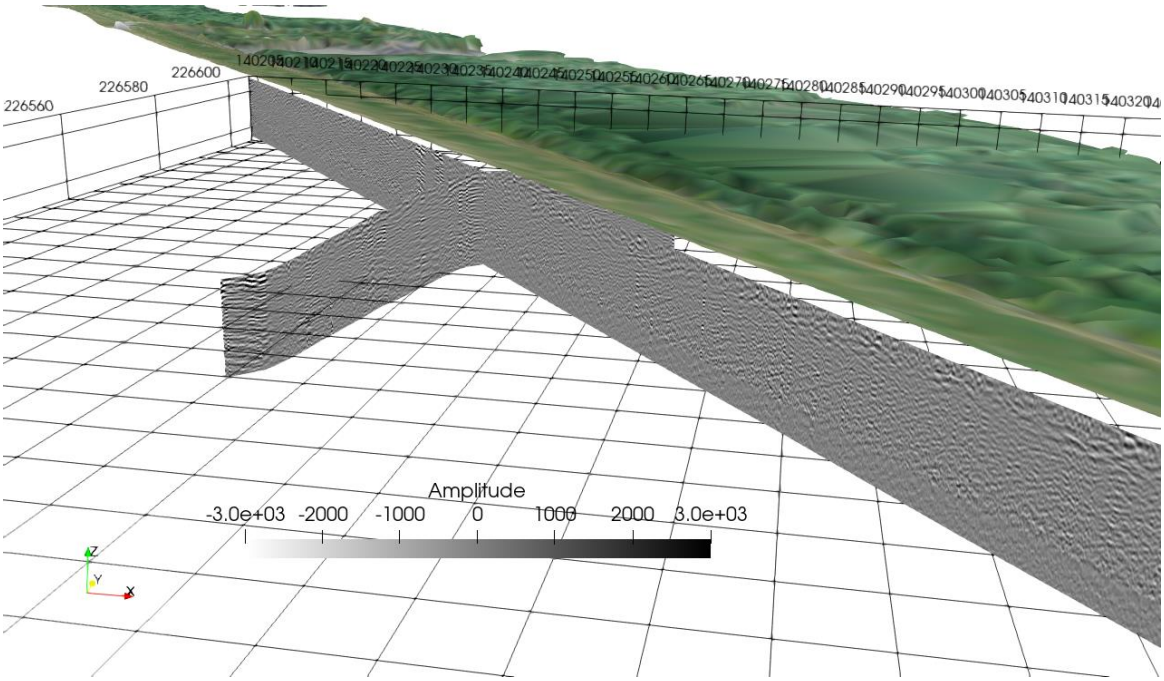

Figure 36: North of the section 6, longitudinal GPR profile GPR_L1_S6 and transverse GPR profile GPR_T23_S6.

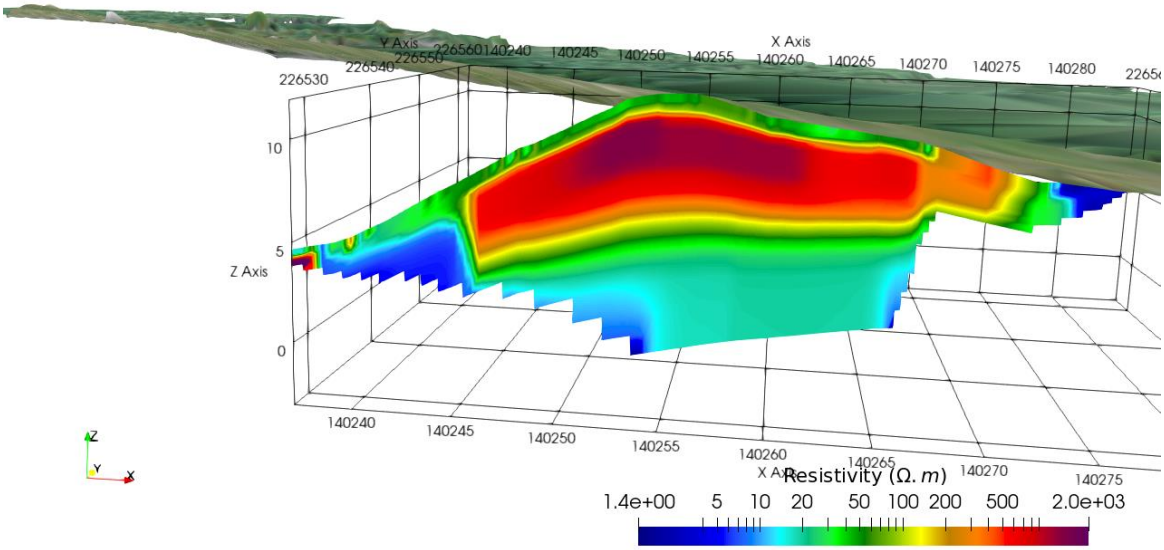

Figure 37: North of the section 6, only transverse profile ERT_T23_S6

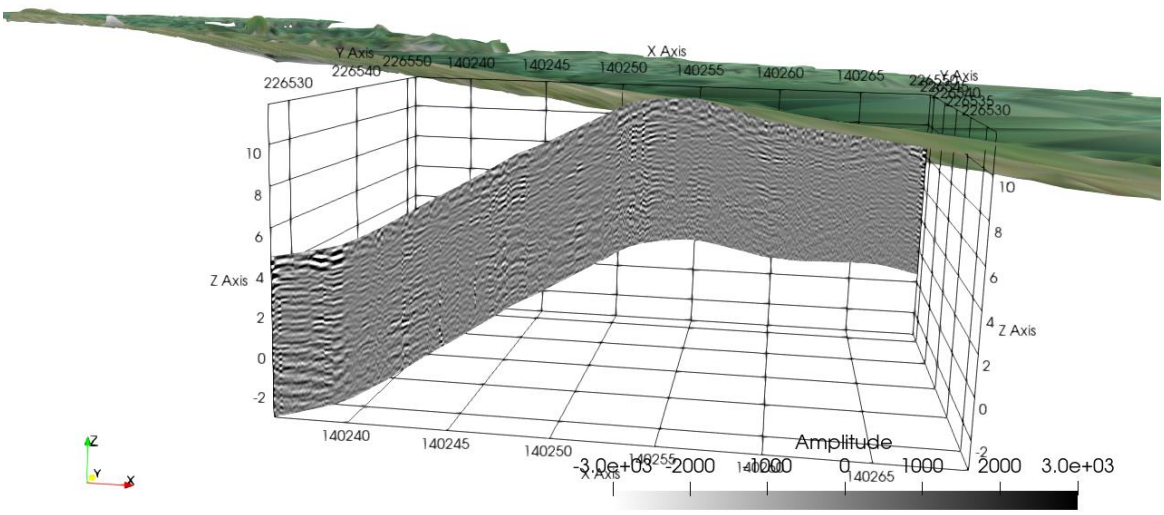

Figure 38: North of the section 6, GPR_T23_S6 transverse profile.

No Permeafor test was performed in the vicinity of the North of the section 6. The nearest CPT is S9 (see Figure 39) and is compared with the ERT_T23_S6 profile (top) and the GPR_T23_S6 profile (bottom). In a similar manner, the qc value depicts the clayey top layer (0 to 1.2 m depth) followed by the dike core (1.2 m to 8.5-9 m depth). The deeper materials over 9 m depth are a mixture of thin layers of silt, silty clay, clay. The CPT is globally well correlated with the ERT measurements.

4.2.3.2 *Comparison of CPT S9, ERT and GPR on section 6, North-West*

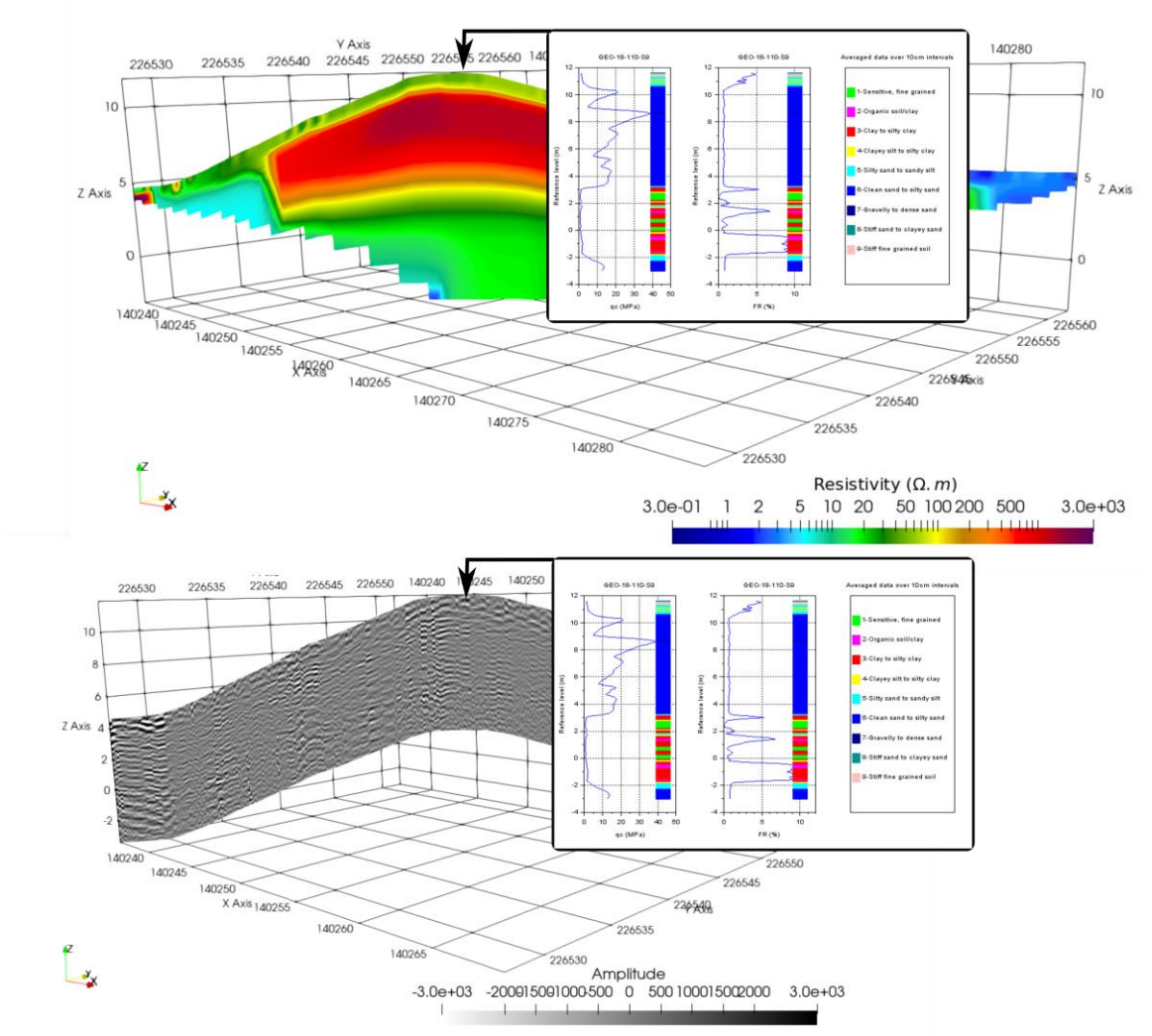

Figure 39: Comparison of CPT S9 interpretation with ERT_T23_S6 profile (top) and GPR_T23_S6 profile (bottom)

4.2.3.3 *Comparison of CPT S8 and S9 with transverse ERT_L2_S6 profile*

We compare here (Figure 40) in the Section 6 the ERT_L2_S6 profile with the CPTs S8 and S9. The ERT (Figure 41 and Figure 42) results globally depict a two-layer structure: the clean to dense sand formation, followed, according to S8 and S9 at 3 m TAW, by a multilayered formation of clayey silt to silty clay and clay to silty clay layers.

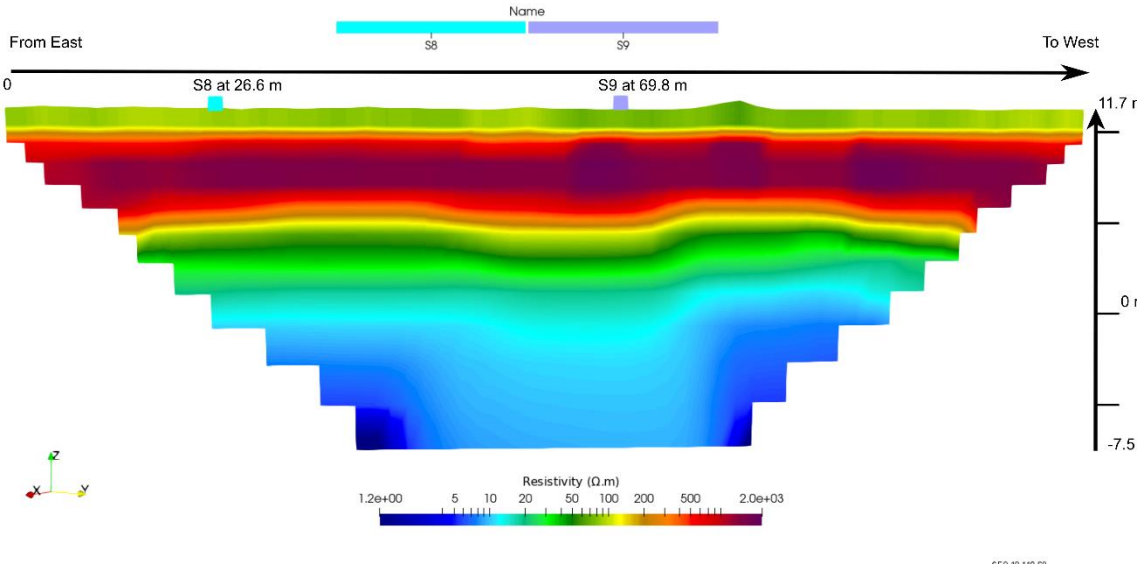

Figure 40: Section 6, North-West, Dutch part with the ERT_L2_S6 profile and the CPTs S8 and S9

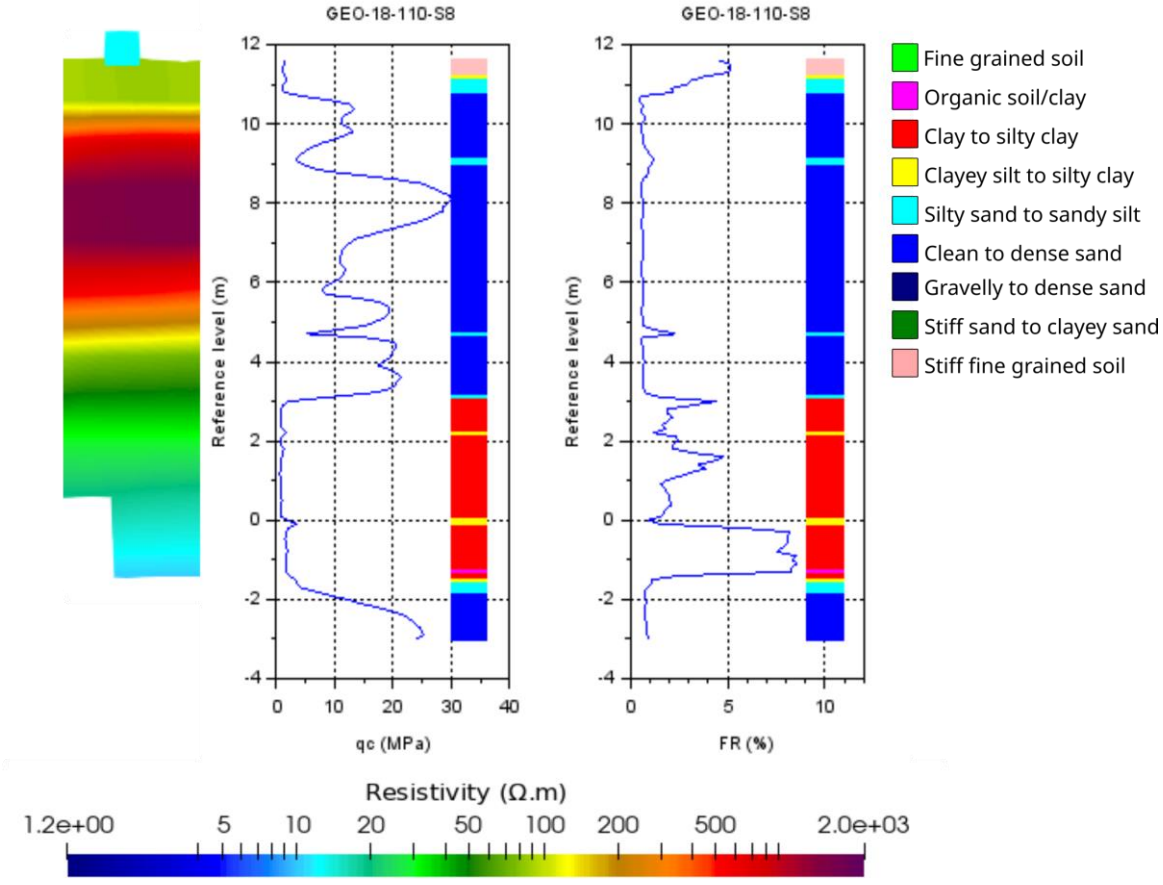

Figure 41 : Resistivity of ERT_L2_S6 profile compared with q_c and R_f at CPT S8

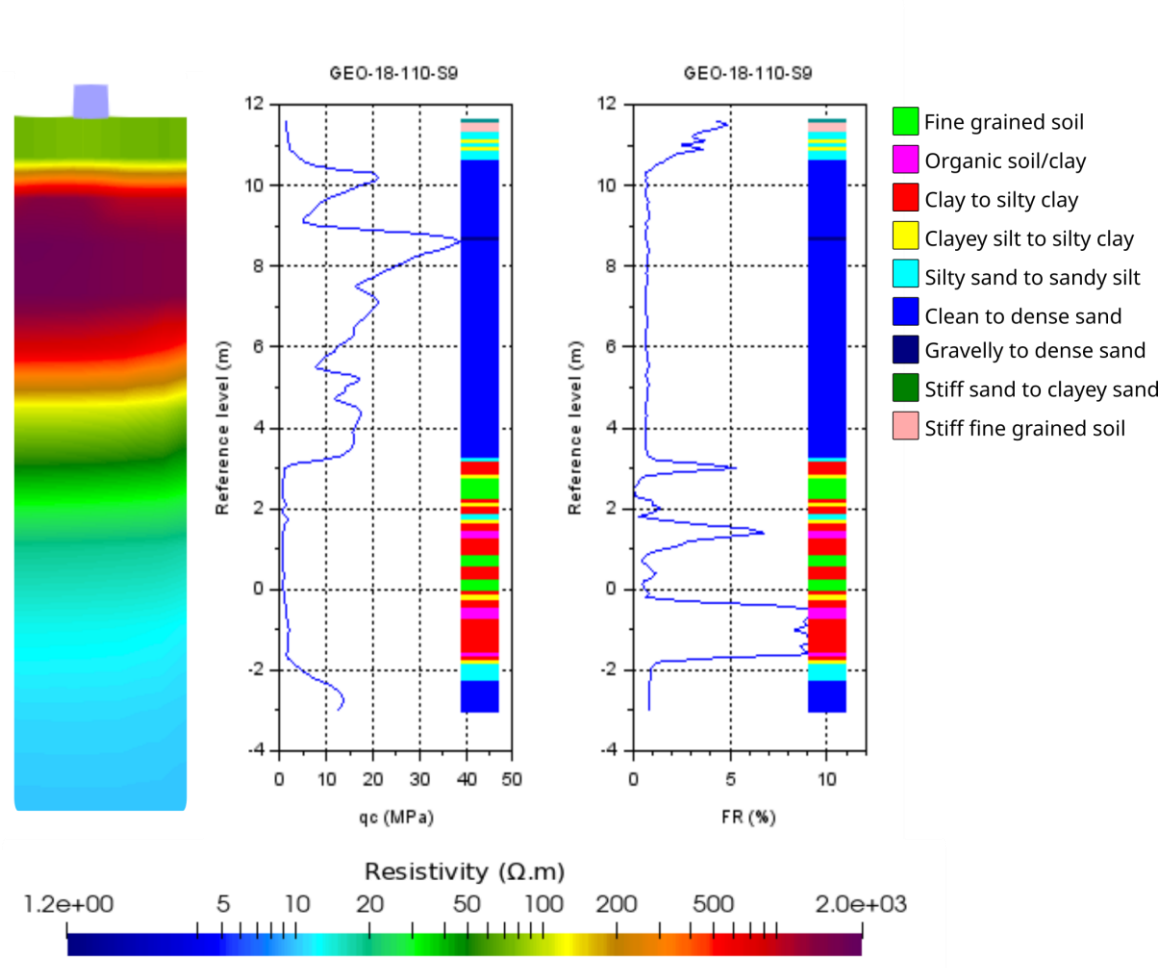

Figure 42: Resistivity of ERT_L2_S6 profile compared with q_c and R_f at CPT S9

4.2.4 Section 10

On section 10 (see Figure 43), only 2 ERT profiles were carried out: the transverse ERT_T24_S10 and the longitudinal ERT_L1_S10. Unfortunately, no CPT nor Permeafor are available. The geophysical analysis doesn't differ from the previous section 6, except for the fact that the resistivity is lower.

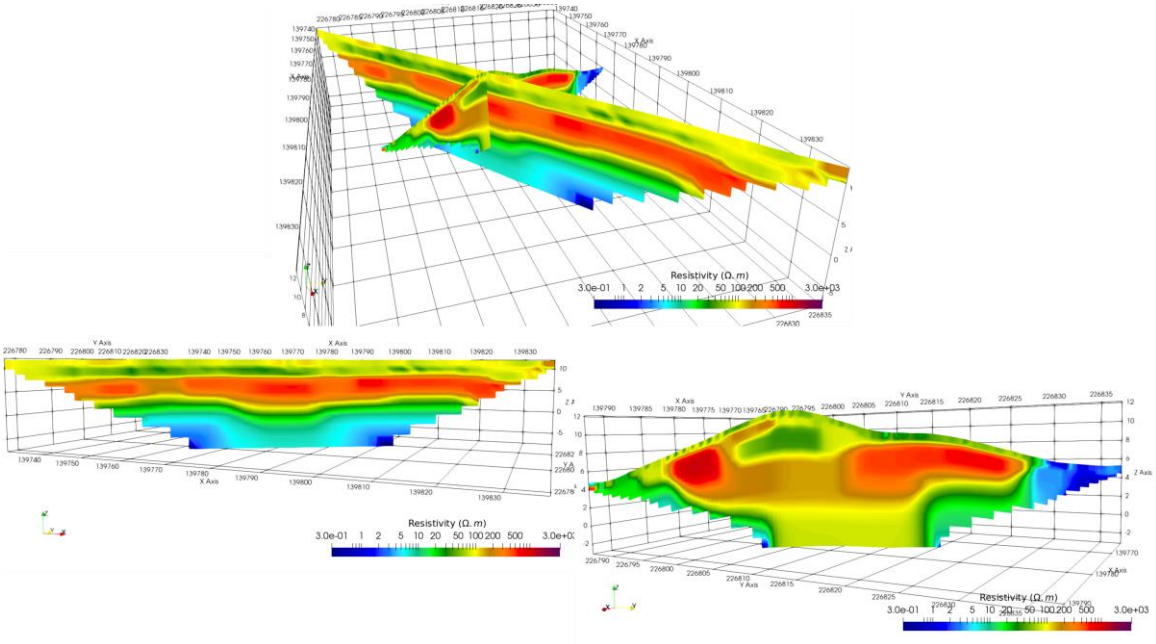

Figure 43: Section 10, the transverse and longitudinal profiles ERT_T24_S10 and ERT_L1_S10, shown together (top); shown individually at the bottom, longitudinal (left), transverse (right),

4.2.5 Section 11

In section 11 (see Figure 44), only one transverse ERT profile was carried out.

A Permeafor PK3_S11 was performed at the crest just left to the road (regarding West direction). The correlation between both methods is obvious when considering the log(Q/H) factor: a clayey top layer of about 1.5-2 m depth, followed by the dike core to 9-10 m depth. (permeability values between 5.10^{-5} and 7.10^{-3} m/s). The density (drilling curve) shows two layers. For the first 6 m below the surface, the density is weak. Below 6 m depth, the density is high. A sublayer is detected between 6 and 10 m depth, with high density and high permeability (approximately 5.10^{-5} to 5.10^{-4} m/s). This could correspond to sandy soils. Between 10 and 12.60 m, the density of the soil is high and the permeability is weak (inferior to 1.10^{-6} m/s). This could correspond to the presence of a fine fraction in the soil.

No CPT testing was performed at the crest.

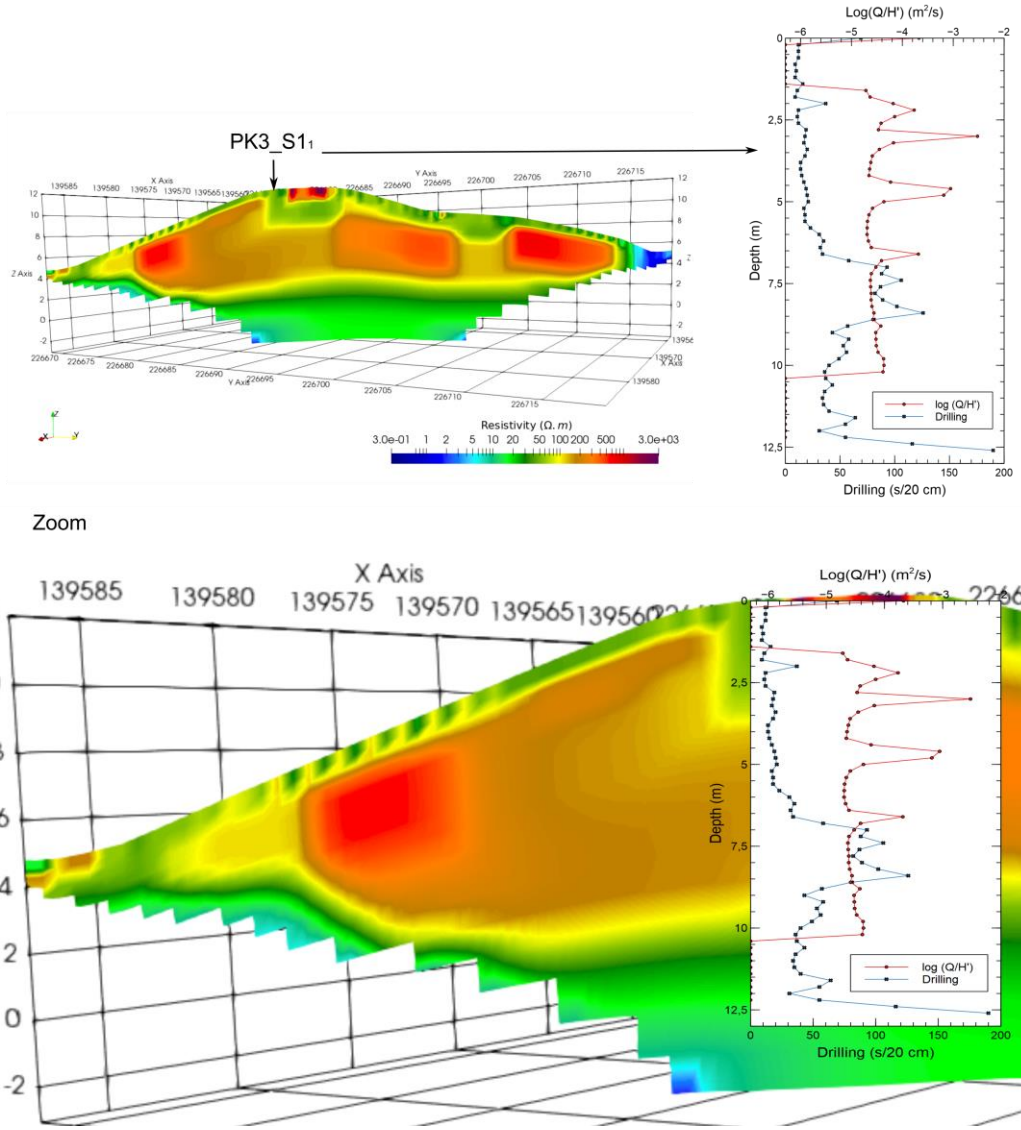

Figure 44: Section 11, only one ERT transverse profile ERT_T25_S11 was performed

4.3 Comparison of 2019 ERT measurements with 2020 ERT measurements

Fugro carried out ERT measurements in 2019 with similar instruments as well as configurations. Fugro already presented a detailed analysis of potential anomalies in the core of the dike.

Cerema's and Fugro's profiles can be compared for the section S4 and S6.

In Section 4 (see Figure 45), the ERT_L1_S4 profile is the longest one, while the ERT2 profile of Fugro represents the beginning (right end on the figure) of the profile. Very similar results are obtained, and the slight differences can be attributed to either different inter-electrode spacing (3 m for Cerema, 2, m for Fugro) or different water content conditions inside the dike between the 2 periods.

In Section 6 (see Figure 46), it is the opposite case: Fugro performed the longest profile while Cerema measurements are located (i) at the beginning of the section (so-called South of section S6) and (ii) at the middle of the section (so-called North of Section 6). The inter-electrode spacing is identical (2 m). Differences between the two measurements are small. ERT profiles are quasi-similar in the South of section 6 (Figure 46, b). In the North of section 6 (Figure 46, c), ERT2 of Fugro shows a noticeable difference in the core dike resistivity at the end of the profile, while the ERT of Cerema doesn't underline this anomaly: indeed, for this later measurement, the depth of investigation at the beginning of the ERT_L1_S6 is too limited. However, the anomaly in the dike crest in the south of section 6 (Figure 46 b) is clearly visible in both ERT profiles, see bright red zone compared to the dark red crest area.

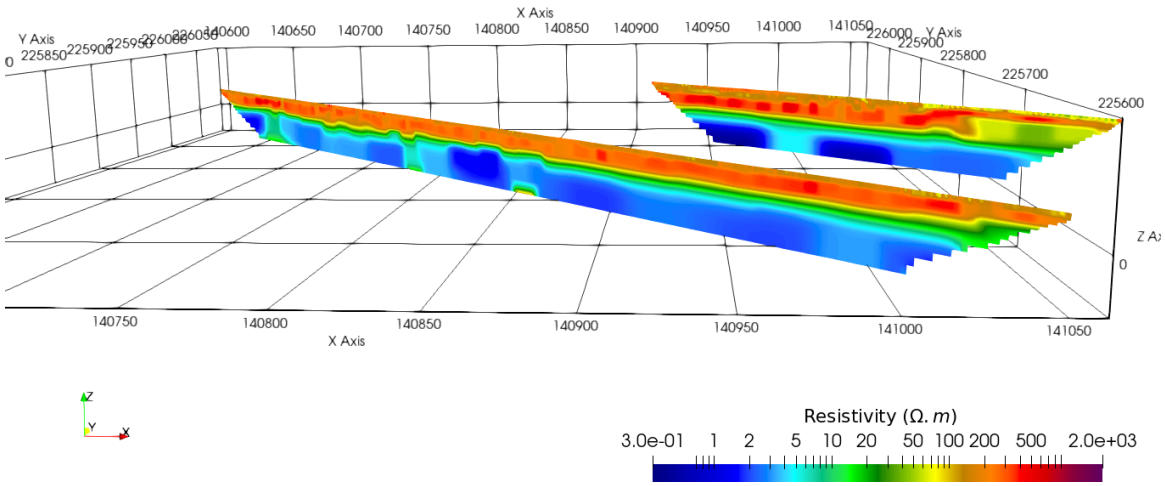

Figure 45: ERT comparison between Fugro-2019 ERT2 profile (top) and Cerema-2020 ERT_L1_S4 (bottom) measurements on section S4, South.

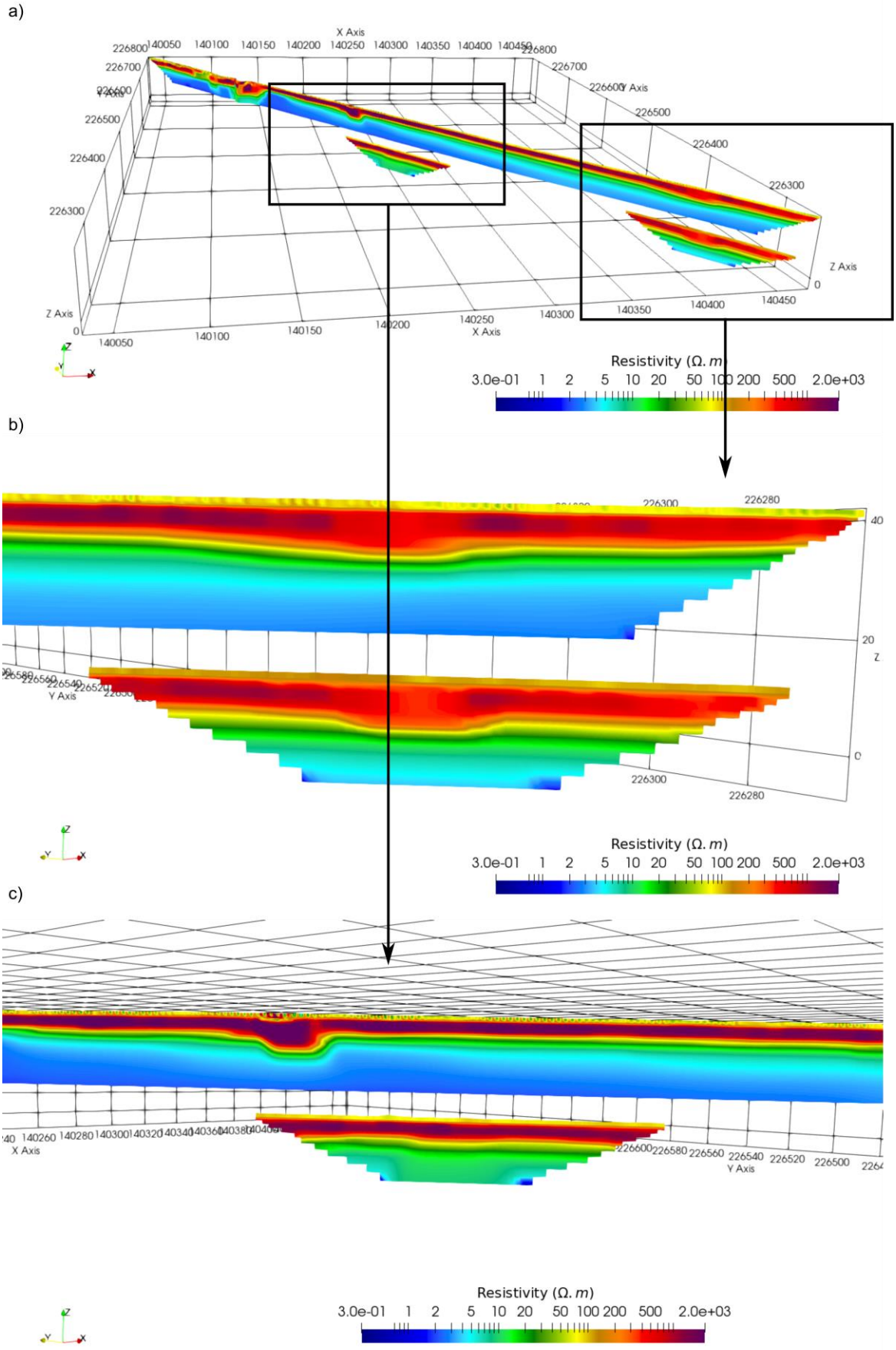

Figure 46: a) ERT comparison between Fugro-2019 ERT1 profile (top) and Cerema-2020 (bottom) measurements on section S6. Zoom on ERT_L1_S6 South (b) and ERT_L2_S6 North (c) of section 6.

4.4 3D effect of the topography

All ERT measurements on section 4, 6 and 10 present longitudinal and transverse profiles on particular locations. We note that the material distribution of the transverse profiles under the crest doesn't match exactly the distribution of materials depicted by the longitudinal profile. For instance, all limits of transverse profiles describing the transition of the clayey top layer with the dike core is slightly lower (~1 m in Dutch part and less than 1 m in Belgian part) than those depicted by longitudinal profiles (See for instance Figure 25).

For transverse cases, ERT configuration and inversion take into account for the topography: each electrode location was measured with DGPS and entered in the RES2DInv software. In that case, the dike is considered as a quasi 2D media, assuming the material distribution doesn't vary between neighboring transverse locations.

On the contrary, the longitudinal profile doesn't take into account for the topography, since inversion is carried out along the profile with the assumption that the surrounding media is at least 2D in (x,y) direction. Consequently, the depth of interface seems to be deeper, as if the topography and the two slopes of the dike limit the vertical resolution.

In conclusion, the 3D effect on 2D-inversed profiles is stronger for longitudinal profiles, and the transverse profiles depict better the transition between the surface clay layer with the sandy core of the dike.

In order to take into account for 3D-topography and to render relevant transverse and longitudinal profile inversion, a solution is to inverse them in the same process, where the topography is included as *a-priori* data. In that purpose, we used a free software developed in Python by Cerema, INSA Rouen and Gustave Eiffel University. It enables to simply input the photogrammetric point cloud and the electrode locations and inverse the ERT data in three dimensions.

An example is given in Figure 47, where all the ERT profiles of section 4 were inversed together. We obtain a 3D-block of resistivity, where particular slices can be achieved in order to represent results in a common manner, i.e. as 2D profiles, such as shown in Figure 47 and Figure 48.

With such processing, there are no more differences between longitudinal and transverse profiles, since they are extracted from a single 3D block of inversed resistivity.

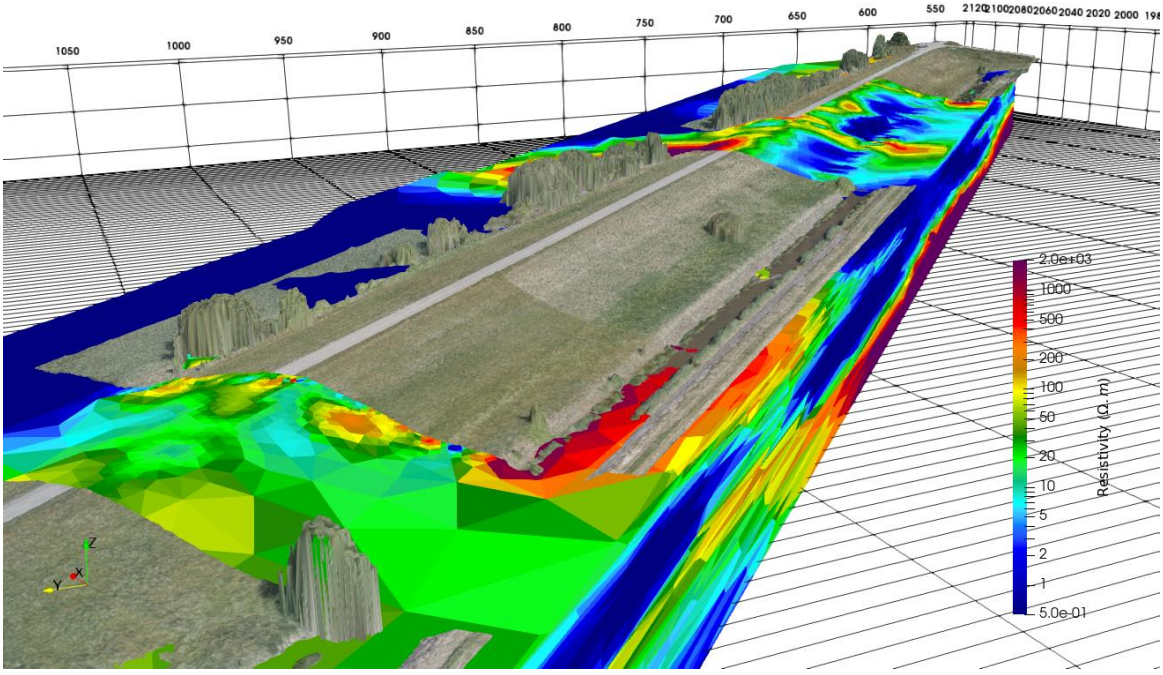

Figure 47: Example of 3D inversion results of all ERT profiles of the section 4.

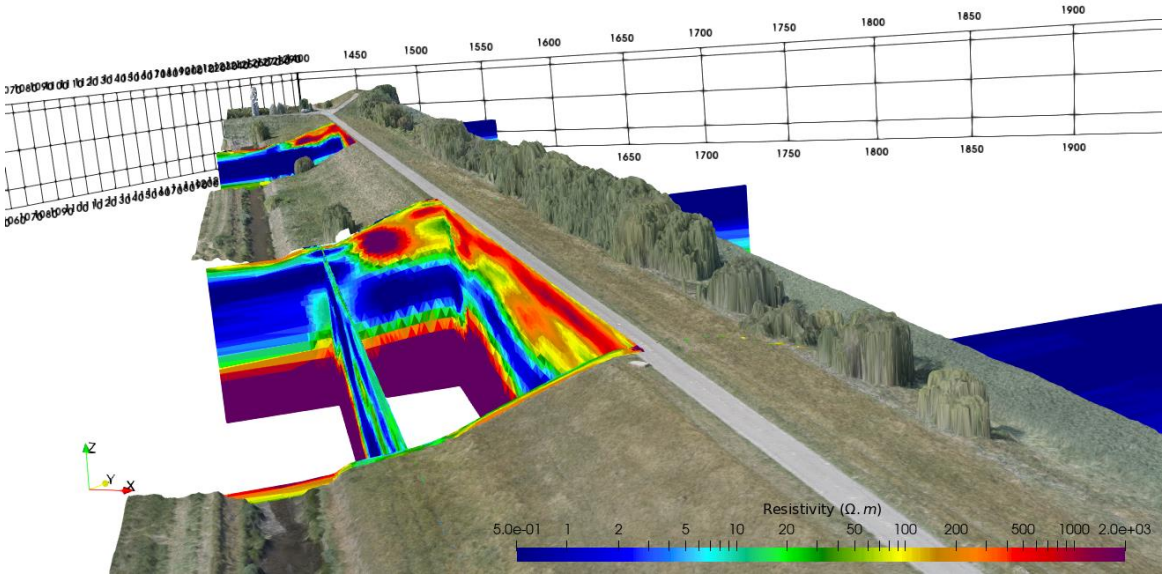

Figure 48: Slices extracted from the 3D ERT block.

5 Conclusion

Geophysical tests, longitudinal and transversal ERT and GPR measurements as well as geotechnical Permeafor tests have been performed by Cerema. Complementary geotechnical measurements: CPTs and drillings with laboratory tests have been performed by the Geotechnics Division of the Flemish Government. The geophysical results have been compared with the geotechnical tests.

The CPTs and the borehole logs offer an accurate description of materials at specific locations. It can be seen that the dike is clearly composed of a clayey top layer with a thickness of about 0.5 to 1.2 m (depending on the location, thinner at the Belgian sections, thicker and less sandy at the Dutch sections). This layer is also well visible on the ERT profiles, as this clayey top layer results in a lower resistivity in the range of 50 to 100 Ω.m, and particularly well defined in the transverse profile, since the electrode spacing is lower (1 m) than in transverse profiles (2 to 3 m) and the 3D topographic effect is lower. Moreover, if a priori the GPR generally exhibits poor results in dike surveys, the method is suitable here since the used frequency (200 MHz) as well as the resistivity of the materials allow for the electromagnetic waves to propagate inside the dike. Nevertheless, while particular anomalies are well identified (road structure in Belgium part and particular features at the bottom of the slopes), an extensive analysis of GPR signals remains to be performed and may be time-consuming.

Underneath the clayey top layer, a sandy core can be found till a depth of 8 to 9 meters. Generally, this layer perfectly fits with a more resistive layer on the ERT profiles of thousands of Ω.m, typical for sandy materials in such a context. Where it is applicable, the Permeafor indicates also the main transition inside the dike.

Below this sandy core the natural subsoil can be found, consisting of a silty/clayey layer with a thickness of 3 to 5 m followed by a peat layer which is generally about 1 to 1.5 m thick. At these levels, ERT shows low resistivities (10 to 20 Ω.m). Underneath the peat layer a sand layer can be found.

It is difficult to distinguish those natural clay and peat layers in the ERT profiles, since the soil is saturated with water. Indeed, in all transverse profiles where the depth of investigation corresponds to these layers, the ERT images show very low resistive layers, typical for very clayey materials or materials containing salt water. From the monitoring well, it was derived that the ground water level was at about 2.5 m TAW in October 2020, when the ERT measurements took place. The presence of this (brackish) water might have influenced the electrical conductivity significantly.

The ERT methods are somehow limited since the layering of the structure is coarsely given in comparison to the CPT results, which give a more detailed layering based on measurements every 2 cm in depth. However, this geophysical method allows for the extension of the interpretation from CPTs which give local point information. Moreover, some anomalies have been underlined thanks to ERT imaging (at the bottom of the slope in the Belgian part as well as in the Dutch part). As far as concerned the outcomes, only three days were required to survey the LLHPP. In conclusion both methods are complementary. The Permeafor tests were locally performed, but the results could only be compared to a limited extent, since only few tests have been done. Nevertheless, the method locally gives a direct assessment of the soil permeability that seems to be consistent with the CPT results.

In the context of the Polder2Cs project, this survey offers an insight of materials that will be involved in following experiments and can contribute to enhance the analysis of the erosion phenomena that are observed during controlled experiments.

6 Acknowledgments

We are very grateful to Davy Depreiter, Bruno Beaucamp, Cyril Ledun and Raphaël Antoine for the geophysical measurements in the field and for their contribution to the *in situ* measurements as well as to the creation of the figures with Paraview and QGIS software.

7 References

Antoine, R., Fauchard, C., Fargier, Y., Durand, E., 2015. Detection of Leakage Areas in an Earth Embankment from GPR Measurements and Permeability Logging. Int. J. Geophys. 2015, 610172. https://doi.org/10.1155/2015/610172

Antoine, R., Fauchard, C., Guilbert, V., Beaucamp, B., Ledun, C., Heinkele, C., Saussaye, L., Muylaert, S., Vancalster, W., Depreiter, D., Sergent, P., 2021. GEOPHYSICAL AND UAV-BASED OBSERVATIONS OVER A FLOOD DEFENSE STRUCTURE: APPLICATION TO THE POLDER2C'S EXPERIMENTAL DIKE. Int. Arch. Photogramm. Remote Sens. Spat. Inf. Sci. XLIII-B3-2021, 237–242. https://doi.org/10.5194/isprs-archives-XLIII-B3-2021-237-2021

Chiaradonna, A., Flora, A., d'Onofrio, A., Bilotta, E., 2020. A pore water pressure model calibration based on in-situ test results. Soils Found. 60, 327–341. https://doi.org/10.1016/j.sandf.2019.12.010

Das, S., Sarkar, S., Kanungo, D.P., 2022. Rainfall-induced landslide (RFIL) disaster in Dima Hasao, Assam, Northeast India. Landslides. https://doi.org/10.1007/s10346-022-01962-z

Dezert, T., Lopes, S.P., Fargier, Y., Côte, P., 2019. Combination of geophysical and geotechnical data using belief functions: Assessment with numerical and laboratory data. J. Appl. Geophys. 170, 103824. https://doi.org/10.1016/j.jappgeo.2019.103824

Fargier, Y., Lopes, S.P., Fauchard, C., François, D., Côte, P., 2014. DC-Electrical Resistivity Imaging for embankment dike investigation: A 3D extended normalisation approach. J. Appl. Geophys. 103, 245–256. http://dx.doi.org/10.1016/j.jappgeo.2014.02.007

Fauchard, C., Fargier, Y., Maquaire, O., Antoine, R., Costa, S., Medjkane, M., Roulland, T., Ledun, C., Guilbert, V., Davidson, R., 2018. Combination of aerial and near surface geophysical data: Badlands case study of "Les Vaches Noires" cliffs, Normandy, France. Eur. Geosci. Union Gen. Assem. 2018 Vienne Austria 8-13 April 2018.

Fauchard, C., Mériaux, P., 2007. Geophysical and geotechnical methods for diagnosing flood protection dikes. Guide for implementation and interpretation. Editions Quae.

Griet De Backer, Stefanie D'heer, 2021. REPORT GEO-18/111. Report on the geotechnical laboratory testing, INTERREG Polder2C's project.

Hennig, T., Weller, A., Canh, T., 2005. The effect of dike geometry on different resistivity configurations. J. Appl. Geophys. 57, 278–292. https://doi.org/10.1016/j.jappgeo.2005.03.001

Imaide, K., Nishimura, S., Shibata, T., Shuku, T., Murakami, A., Fujisawa, K., 2019. Evaluation of liquefaction probability of earth-fill dam over next 50 years using geostatistical method based on CPT. Soils Found. 59, 1758–1771. https://doi.org/10.1016/j.sandf.2019.08.002

Larrabee, A. C., 2010. Determination of hydraulic conductivity using the Perméafor. Master's Thesis, University of New Hampshire, Durham, USA.

Larrabee, A. C., Benoît, J., Reiffsteck, Ph., 2012. Profiling hydraulic conductivity in situ. Geotechnical and Geophysical Site Characterization 4. Coutinho & Mayne (eds), 1:545-552.

Liao, T., Mayne, P.W., Tuttle, M.P., Schweig, E.S., Arsdale, R.B.V., 2002. CPT site characterization for seismic hazards in the New Madrid seismic zone. Soil Dyn. Earthq. Eng. 22, 943–950. https://doi.org/10.1016/S0267-7261(02)00118-5

Loke, M., 2004. Tutorial: 2-D and 3-D electrical imaging surveys.

Marescot, L., Rigobert, S., Lopes, S.P., Lagabrielle, R., Chapellier, D., 2006. A general approach for DC apparent resistivity evaluation on arbitrarily shaped 3D structures. J. Appl. Geophys. 60, 55–67. https://doi.org/10.1016/j.jappgeo.2005.12.003

Pierrot-Deseilligny, M., Clery, I., 2012. Some possible protocols of acquisition for optimal use of the "APERO" open source software in automatic orientation and calibration, in: Castelldefels, Spain, Tutorial, EuroCOW Workshop. pp. 8–10.

Reiffsteck, Ph., Dorbani, B., Khay, M., Haza-Rozier, E., 2009. Appareillage pour diagraphie de perméabilité. 17th International Conference on Soil Mechanics and Geotechnica (ICSMGE), Alexandria, Egypt, October 5-9, 2009,

Reiffsteck, Ph., Dorbani, B., Haza-Rozier, E., Fry, J.-J., 2010. A new hydraulic profiling tool including CPT measurements, in: 2nd International Symposium on Cone Penetration Testing : CPT'10, Huntington Beach, CA, May 9-11, 2010 : Conference Proceedings. [CPT'10 Organizing Committee].

Rücker, C., Günther, T., Spitzer, K., 2006. Three-dimensional modelling and inversion of dc resistivity data incorporating topography - I. Modelling. Geophys. J. Int. 166, 495–505.

Sharp, M., Wallis, M., Deniaud, F., Hersch-Burdick, R., Tourment, R., Matheu, E., Seda-Sanabria, Y., Wersching, S., Veylon, G., Durand, E., Smith, P., Forbis, J., Spliethoff, C., van Hemert, H., Igigabel, M., Pohl, R., Royet, P., Sharp, M., Simm, J., Tourment, R., Wallis, M., 2013. The International Levee Handbook. CIRIA.

Telford, W.M., Geldart, L.P., Sheriff, R.E., 1990. Applied Geophysics, 2nd ed. Cambridge University Press, Cambridge. https://doi.org/10.1017/cbo9781139167932

Tsai, C.-C., Yang, Z.-X., Chung, M.-H., Hsu, S.-Y., 2022. Case study of large-scale levee failures induced by cyclic softening of clay during the 2016 Meinong earthquake. Eng. Geol. 297, 106518. https://doi.org/10.1016/j.enggeo.2022.106518

Wuebbolt, S. L., 2020. Profiling of hydraulic conductivity using a Permeafor. Master's Theses and Capstones, University of New Hampshire.

Zhdanov, M.S., Keller, G.V., 1994. The geoelectrical methods in geophysical exploration, Elsevier. ed, Methods in geochemistry and geophysics. Elsevier.

8 Appendix

As discussed in the report, we tried to compare the Perméafor with the CPT measurements. We obtain curves with similarities, however with a systematic offset in depth of approximately 50cm. Unfortunately, at this stage we were unable to unequivocally determine the cause or provide a plausible explanation. For information, the comparison is presented here in this Appendix.

The Permeafor

The Permeafor aims at evaluating hydraulic conductivity in situ, rapidly (vertical diagraphy). The tool is approximately 80 cm in length and 5 centimeters in diameter with a perforated section at the center of the probe. The tapered design forces the flow of water out of the perforated section in the radial direction. The conical tip allows the probe to be inserted in the ground using a percussion drill rig. It is specifically designed to test lateral hydraulic conductivity. The Permeafor probe is shown in Figure 49.

Figure 49: Permeafor probe

At testing intervals of 20 cm, the advance is stopped and the flow is monitored for 10 seconds before proceeding to the next test depth. The flow of water, Q (m^3/s), is measured at the surface. As water flows through the tubing to the probe, head losses (dH) occur due to friction. Head losses are also present in the flow meter and the tubing connections. The effective head, H' (m), is then reported which is a function of the pressure head and the pressure losses. Results from testing with the probe are reported for each test depth as a ratio of the flow to the effective head, Q/H' (m^2/s) along with the penetration effort to advance the probe. The values of Q/H' are bounded at 1.10^{-3} and 1.10^{-6} m^2/s. A full profile can be carried out in a few hours.

The measurements obtained during testing with the Permeafor can be correlated to hydraulic conductivity (Larrabee et al., 2012):

$$k\left(\frac{m}{s}\right) = \left(Q/H'\right) * \left(1/(7.02 * 0.05)\right) = 2.8\left(Q/H'\right)$$

The expected result is a quasi-continuous log illustrating the in-situ hydraulic conductivity and density of the crossing material allowing the assessment of the levee structure and its natural subsoil and a detection of leaks.

Comparison between Permeafor and CPTs results on the section 4

Unfortunately at this location, the Permeafor testing stopped at 6 m depth. Nevertheless, as depicted in Figure 50 there is a good but 50cm-offset correlation between Permeafor factors (drillings (s/20cm) and log(Q/H) (m^2/s)) and CPT measurements (qc(MPa), fs(MPa) and the ratio fs/qc = Rf (%)). Indeed, the peaks in resistance (drilling curve of the Permeafor and qc curve of the CPT, even if the two parameters correspond to different mechanical solicitation) are recorded at the

same depths. The transmissivity (log (Q/H') curve of the Permeafor) peaks are located at 1,60 m depth (3.10^{-6} m²/s, which corresponds approximately to a permeability of 9.10^{-6} m/s), between 4,00 and 4,60 m depth (5.10^{-6} to 1.10^{-5} m²/s or approximately 1 to 3.10^{-5} m/s) and between 5,20 and 5,40 m depth (9.10^{-6} to 1.10^{-5} m²/s or approximately 2 to 3.10^{-5} m/s). For all other depths, the transmissivity log indicates a constant permeability of the soils lower than 1.10^{-6} m/s, which is the low measuring bound of the Permeafor. These permeability values are plausible for a clean to dense sand of a dike core.

The resistance measured with PK4_Sect4 and PK6_Sect4 shows similar results to a depth of 6 m. The permeability values reached 2.10^{-4} m/s at 3,40 m depth in the PK4_Sect4 drill and 1.10^{-3} m/s at 2,00 m depth in the PK6_Sect4 drill. Below 6 m depth, in PK6_Sect4, permeability peaks of 2.10^{-5} to 2.10^{-4} m/s are detected between 7.40 and 8.40 m depth. It could correspond to sand material.

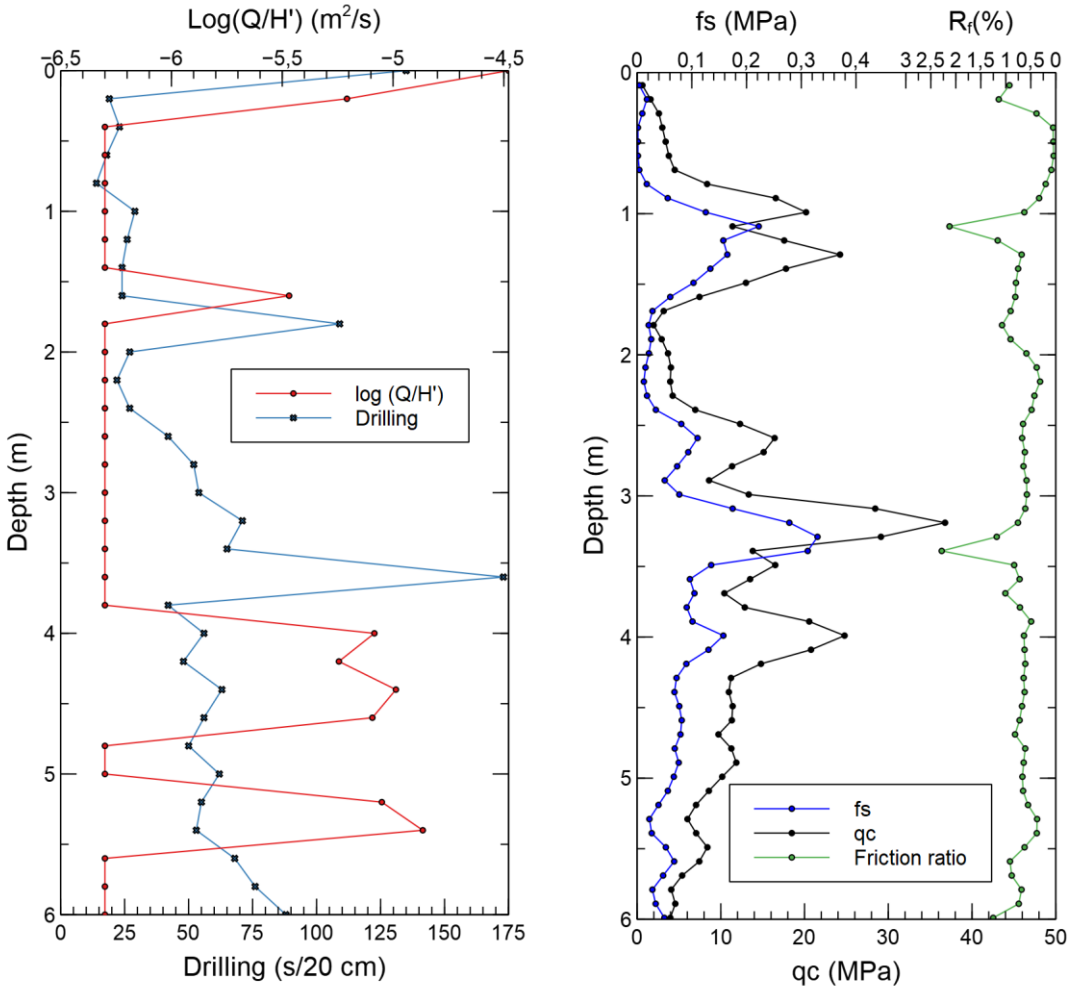

Figure 50: Comparison between CPT S18 and Permeafor Pk3_Sect4 on the section 4. Both drillings were performed at a very close location of the ERT_T10_S4 and GPR_TA0_4. Permeafor stopped at 6 m depth while CPT continued till 16 m depth.

As far as concerned, the nature of materials, the CPT parameters (see colored legend of Figure 50**Erreur ! Source du renvoi introuvable.**) as well as the drilling B18B (Figure 16) show that the first six meters below the surface of the crest are mainly composed of sandy materials.

Comparison between CPT S1 and Permeafor PK8_S4

For this section (see Figure 51) we consider the ERT profile ERT_L1_S6 and the CPT S1 and Pk8_S6 Permeafor. In this case, for the Permeafor, the resistance (drilling curve) is weak for the first 6 m below the surface. Then, it increases up to 8.5 m depth and indicates important peaks between 8.50 and 12.20 m depth. The peaks of the qc curve of the CPT S1 indicate high resistance between 1 and 2 m depth, then between 5 and 9 m depth, in clean to dense sand. So, the resistance values of the two drilling types are not perfectly correlated.

The transmissivity (log (Q/H') curve) of the soils is important for the first 6 m below the surface, with values between 6.10^{-6} and 1.10^{-3} m²/s (or permeability values between 1.10^{-5} and 3.10^{-3} m/s). This corresponds to the dike sand core. The presence of a fine fraction between 3 and 4 m depth, as can be noticed in the CPT diagram, is not detected.

Deeper than 6 m , the transmissivity values are weaker than 5.10^{-7} m²/s (or 1.10^{-6} m/s), which is the lower limit of measurements of the Permeafor, with only some peaks at 6.40-6.60, 7.20-7.60, 8.00, 11.00 and 11.40 m depth, between 2.10^{-6} and 5.10^{-5} m²/s (or between 6.10^{-6} and 1.10^{-4} m/s). These peaks could correspond to sandy passes into clay to silty clay.

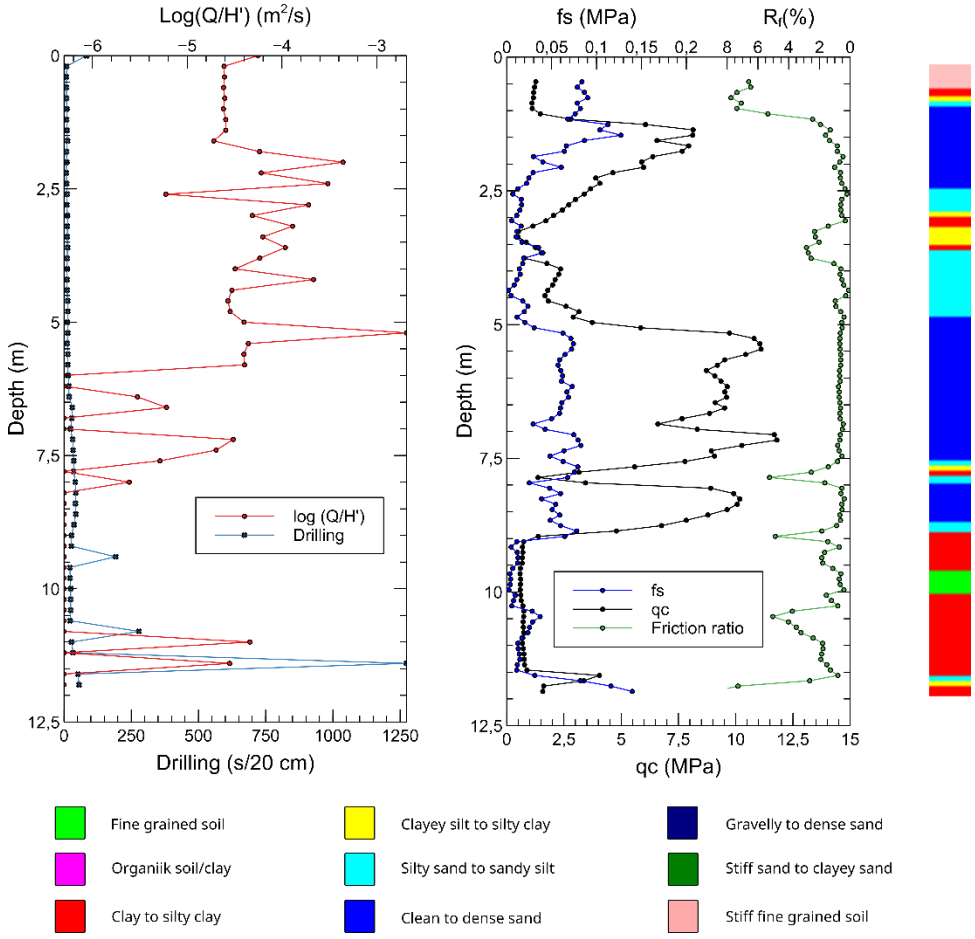

Figure 51: Comparison between CPT S1 and Permeafor PK8_S6